# G-baToN: a versatile reporter system for cancer cell-stromal cell interactions

Rui Tang[1*], Christopher W. Murray[2], Ian Linde[4], Nicholas J. Kramer[1,3], Zhonglin Lyu[6], Min K. Tsai[1], Leo Chen[1], Hongchen Cai[1], Aaron D. Gitler[1,3], Edgar Engleman[2,4,5], Wonjae Lee[6], and Monte M. Winslow[1,2,5*]

[1] Department of Genetics, Stanford University School of Medicine, Stanford, CA, USA

[2] Cancer Biology Program, Stanford University School of Medicine, Stanford, CA, USA

[3] Neuroscience Program, Stanford University School of Medicine, Stanford, CA, USA

[4] Immunology Program, Stanford University School of Medicine, Stanford, CA, USA

[5] Department of Pathology, Stanford University School of Medicine, Stanford, CA, USA

[6] Department of Neurosurgery, Stanford University School of Medicine, Stanford, CA, USA

* Corresponding authors: Rui Tang: tangrui@stanford.edu and Monte M. Winslow: mwinslow@stanford.edu

## ABSTRACT

Cell-cell interactions influence all aspects of development, homeostasis, and disease. In cancer, interactions between cancer cells and stromal cells play a major role in nearly every step of carcinogenesis. Thus, the ability to record cell-cell interactions would facilitate mechanistic delineation of the role of cancer microenvironment. Here, we describe GFP-based Touching Nexus (G-baToN) which relies upon nanobody-directed fluorescent protein transfer to enable sensitive and specific labeling of cells after cell-cell interactions. G-baToN is a generalizable system that enables physical contact-based labeling between various cell types, including diverse cancer-stromal cell pairs. A suite of orthogonal baToN tools enables reciprocal cell-cell labeling, interaction-dependent cargo transfer, and the identification of higher-order cell-cell interactions across a wide range of cell types. The ability to track physically interacting cells with these

simple and sensitive systems will greatly accelerate our understanding of the outputs of cell-cell interactions in cancer as well as across many biological processes.

## INTRODUCTION

Cell-cell interactions contribute to almost all physiological and pathological states(Deb, 2014; Komohara and Takeya, 2017; Konry et al., 2016; Zhang and Liu, 2019). Despite the explosion of interest in uncovering and understanding cellular heterogeneity in tissues and across disease states, the extent to which cell-cell interactions influence cell state, drive heterogeneity, and enable proper tissue function remains poorly understood (Konry et al., 2016; Tsioris et al., 2014; Zhang and Liu, 2019). Detailed analysis of the impact of defined cell-cell interactions has illuminated critical aspects of biology, however, these analyses have been limited to a small number of juxtacrine signaling axes that are tractable to study (Dustin and Choudhuri, 2016; Meurette and Mehlen, 2018; Yaron and Sprinzak, 2012).

Interactions between cancer cells and stromal cells play a central role in cancer initiation, progression, and metastasis (Kitadai, 2010; Orimo and Weinberg, 2006). While secreted factors relaying pro- or anti-tumor signals have been extensively investigated, the impact of direct physical interactions between cancer cells and stromal cells remains understudied (Bendas and Borsig, 2012; Dittmer and Leyh, 2014; Nagarsheth et al., 2017). A greater understanding of the constellation of direct interactions that cancer cells undergo will not only deepen our understanding of tumor ecology but also has the potential to uncover novel therapeutic opportunities (Nagarsheth et al., 2017; Swartz et al., 2012). Furthermore, how diverse cell-cell interactions differentially impact cancer cells at different stages of carcinogenesis and within different organ environment remains largely uncharacterized.

50 Molecular methods to profile cell state, including *in situ* approaches within intact tissues,
51 largely fail to uncover the causal relationship between cell-cell interactions and the underlying
52 biology (Giladi et al., 2020; Halpern et al., 2018). Computational and experimental methods to
53 characterize cell-cell interactions yield additional layers of dimensionality, however, modalities
54 to capture cell-cell interactions are limited (Boisset et al., 2018; Morsut et al., 2016; Pasqual et
55 al., 2018). Much as diverse systems to detect and quantify protein-protein interactions have
56 revolutionized our biochemical understanding of molecular systems, the development of novel
57 systems to detect and quantify cell-cell interactions will accelerate the mapping of the interaction
58 networks of multicellular systems.
59 Endogenous cell-cell interactions can result in transfer of surface proteins between cells,
60 mainly through either trans-endocytosis or trogocytosis (Langridge and Struhl, 2017; Li et al.,
61 2019; Ovcinnikovs et al., 2019). Thus, we sought to integrate this phenomenon with fluorescent
62 protein tagging to label cells that have undergone direct interactions. We describe a surprising
63 robust system (which we term GFP-based Touching Nexus or G-baToN) that enables sensitive
64 and specific interaction-dependent labeling of cancer cells and various primary stromal cells,
65 including endothelial cells, T cells and neurons. We extensively characterize this approach and
66 describe several novel applications of this versatile system.
67
68 **RESULTS**
69
70 **G-baToN enables cell-cell interaction-dependent labeling**
71 To create a system where a fluorescent signal could be transferred between neighboring
72 cells, we adapted a synthetic ligand-receptor system based on the expression of surface GFP

73 (sGFP) on sender cells and a cell surface anti-GFP (αGFP) nanobody on receiver cells (Fridy et
74 al., 2014; Lim et al., 2013; Morsut et al., 2016). Co-culturing sGFP sender cells with αGFP
75 receiver cells led to GFP transfer and labeling of the receiver cells (Figure 1A, B and
76 supplementary Figure 1A). Receiver cell labeling required direct cell-cell contact, active
77 membrane dynamics, and pairing between sGFP and its cognate αGFP receptor (Figure 1C, D
78 and Supplementary Figure 1B, C). Notably, sGFP transfer was accompanied by reduced GFP on
79 the sender cells, downregulation of αGFP from the surface of the receiver cells and was partially
80 blocked by chemical inhibitors of endocytosis – all consistent with active GFP transfer and
81 internalization into receiver cells (Supplementary Figure 1D-F).
82 To characterize the kinetics of G-baToN-mediated receiver cell labeling, we performed
83 co-culture time course experiments with time-lapse imaging and flow cytometry readouts. Time-
84 lapse imaging showed rapid transfer and internalization of GFP by receiver cells (Figure 1E and
85 Supplementary Movie 1). GFP transfer could be detected within five minutes of co-culture and
86 was half-maximal after six hours (Figure 1F and Supplementary Figure 1G). Importantly, GFP
87 fluorescence in receiver cells decayed rapidly after isolation of touched receiver cells from
88 sender cells, thus documenting the transient labeling of receiver cells (Supplementary Figure
89 1H). To determine the sensitivity of this system, we co-cultured receiver cells with different
90 ratios of sender cells. The fraction of labeled receiver cells was proportional to the number of
91 sender cells, and even the addition of very few sender cells (representing less than one sender
92 cell to $10^5$ receiver cells) was sufficient to label rare receiver cells (Figure 1G, H). Thus, the
93 transfer of GFP to αGFP-expressing cells is a rapid and sensitive method to mark cells that have
94 physically interacted with a predefined sender population.
95

96 **Fluorescence transfer efficiency is modulated by transmembrane domains and nanobody**
97 **affinity**

98 To further characterize the interaction reporter system, we deconstructed the G-baToN
99 design into three functional modules: 1) the transmembrane domain of αGFP on receiver cell; 2)
100 the pairing between GFP and αGFP; and 3) the transmembrane domain of sGFP on sender cell.
101 We initially used a published sGFP-αGFP pair which used the Notch1 transmembrane domain to
102 link the LaG17-αGFP nanobody onto the receiver cell and the PDGFR transmembrane domain
103 to link sGFP onto the sender cell (Morsut et al., 2016). Replacement of the Notch1
104 transmembrane domain of αGFP with different transmembrane domains allowed us to quantify
105 their impact on GFP transfer efficiency. The VEGFR2 transmembrane domain enabled the
106 highest transfer efficiency, resulting in about a three-fold increase relative to the original design
107 (Figure 2A-C). We next replaced the LaG17-αGFP nanobody with αGFP nanobodies with
108 varying affinity for GFP (Figure 2D, E). While nanobodies exhibiting the highest affinities
109 performed similarly, we noted a minimal affinity required for GFP transfer (Figure 2F). Overall,
110 the efficiency of GFP transfer correlated with GFP affinity. Lastly, permutation of
111 transmembrane domain of sGFP on the sender cell revealed that the rate of retrograde transfer of
112 αGFP-VEGFR2-BFP from receiver to sender cells was influenced by the sGFP transmembrane
113 domain (Figure 2G-I). The PDGFR transmembrane domain minimized bidirectional transfer and
114 thus was the optimal design for minimizing retrograde transfer which could generate false-
115 positive signals (Figure 2G-I). Collectively, the permutation of the transmembrane domains
116 anchoring sGFP and αGFP, as well as varying the αGFP nanobody affinity enabled the
117 identification of designs that maximize unidirectional receiver cell labeling.
118

119 **Tracking cancer-stroma interactions using G-baToN**

120 Cancer cells interact with a variety of stromal cells at both the primary and metastatic
121 sites (Kota et al., 2017; Nielsen et al., 2016). Thus, we employed the G-baToN system to record
122 various cancer-stroma interactions in conventional 2D and 3D microfluidic culture systems as
123 well as *in vivo*. Co-culturing sGFP-expressing lung adenocarcinoma cells with primary human
124 umbilical vein endothelial cells (HUVECs) in a 2D format led to robust endothelial cell labeling
125 (Figure 3A, B). Additionally, within 3D microfluidic chips, pre-seeded HUVECs expressing
126 αGFP were robustly labeled following co-incubation with sGFP-expressing lung
127 adenocarcinoma cells over a 24-hour period (Figure 3E-G). Thus, the G-baToN system is able to
128 efficiently record cancer cell-endothelial cell interactions across multiple culture conditions.

129 Given the importance of interactions with adaptive immune cells during carcinogenesis
130 (Crespo et al., 2013; Joyce and Fearon, 2015), we assessed the ability of the G-baToN system to
131 track the interaction of primary human CD4 and CD8 T cells with lung cancer cells. αGFP-
132 expressing CD4 and CD8 T cells that interacted with sGFP-expressing lung cancer cells in
133 culture were specifically labeled (Figure 4A-C). To test the ability of the G-baToN system to
134 capture cancer cell-T cell interactions *in vivo*, we established lung tumors from a sGFP-
135 expressing lung adenocarcinoma cell line prior to intravenous transplantation of αGFP-
136 expressing CD4 T cells. 24 hours after T cell transplantation, over 60% of αGFP-expressing
137 CD4 T cells within the tumor-bearing lungs were labeled with GFP, while control CD4 T cells
138 remained unlabeled (Figure 4D, E). Thus, the G-baToN system is capable of recording cancer
139 cell-T cell interactions both *in vitro* and *in vivo*.

140 Recent studies have demonstrated a supportive role for neurons within the primary and
141 metastatic niche in the context of brain (Venkatesh et al., 2019; Zeng et al., 2019). To record

142 cancer cell-neuron interactions, we co-cultured sGFP-expressing lung adenocarcinoma cells with
143 primary cortical neurons expressing αGFP. Physical contact between cancer cells and neuronal
144 axons led to punctate-like GFP granule transport into receiver neuron (Figure 5A-B). These
145 results demonstrate the successful application of G-baToN system to record a variety of cancer
146 cell-stromal cell interactions.
147
148 **G-baToN can be applied in a wide range of cell types**
149 To assess the generalizability of the G-baToN system across cell types, we expressed
150 αGFP in a panel of cell lines and primary cells. Each receiver cell type was able to uptake GFP
151 from sGFP-expressing lung cancer sender cells upon cell-cell contact (Supplementary Figure
152 2A). Furthermore, diverse cancer cell lines and primary cell types expressing sGFP were able to
153 transfer GFP to αGFP-expressing HEK293 receiver cells (Supplementary Figure 2B-F). As
154 anticipated, receiver cell labeling required sGFP-expression on the sender cell and αGFP
155 expression on the receiver cells. Thus, G-baToN-based labeling extends beyond transformed cell
156 types and can label diverse primary cell types in co-culture.
157 To further test the generalizability of the system and determine whether primary cells can
158 serve as both sender and receiver cells, we assessed GFP transfer between interacting primary
159 cells in the context of two well-established heterotypic cell-cell interactions: endothelial cells
160 interacting with smooth muscle cells and astrocytes interacting with neurons. Co-culturing sGFP-
161 expressing HUVEC and αGFP-expressing primary human umbilical vein smooth muscle cells
162 (HUVSMC) resulted in efficient receiver smooth muscle cell labeling (Figure 3C,D).
163 Furthermore, sGFP-expressing astrocytes were able to transfer GFP to αGFP-expressing cortical

164 neurons (Figure 5C, D). Collectively, these results document the efficiency of G-baToN-based
165 cell labeling across diverse cell types.
166
167 **Implementation of multicolor labeling enables recording of reciprocal and higher-order**
168 **interactions**
169 Given the high efficiency with which sGFP labels receiver cells upon interaction with
170 cognate sender cells, we tested whether other surface antigen/antibody pairs could lead to protein
171 transfer and labeling. Due to the cross reactivity of αGFP with BFP, co-culture of surface BFP
172 (sBFP) sender cells with αGFP receiver cells generated BFP-labeled receivers (Fridy et al.,
173 2014) (Supplementary Figure 3A, B). Orthogonal systems consisting of surface-
174 mCherry/αmCherry (LaM4)(Fridy et al., 2014) and surface-GCN4-GFP/αGCN4 (single-chain
175 variable fragment, scFV)(Tanenbaum et al., 2014) also led to efficient and specific receiver cell
176 labeling (Supplementary Figure 3C-F). Thus, the G-baToN labeling system can be extended to
177 additional antigen/antibody pairs.
178 We next integrated these orthogonal systems to enable reciprocal labeling and detection
179 higher order multi-cellular interactions. Engineering cells with these orthogonal systems in an
180 anti-parallel fashion should enable reciprocal labeling of both interacting cells. Co-culture of
181 cells expressing sGFP and αmCherry with cells expressing smCherry and αGFP resulted in
182 reciprocal labeling of both interacting cell types (Figure 6A, B, Supplementary Figure 4A). This
183 reciprocal labeling system may be particularly useful when the interaction induces alteration in
184 both interacting cell types. Using orthogonal ligand-receptor pairs, we also created an AND gate
185 dual labeling strategy. Specifically, co-expression of αmCherry and αGFP on receiver cells
186 enabled dual color labeling of receiver cells that had interacted with smCherry-expressing,

187 sGFP-expressing, or both sender cell types (Figure 6C, D, Supplementary Figure 4B).
188 Analogously, we achieved dual color labeling of receiver cells by leveraging the ability of αGFP
189 to bind both sGFP and sBFP (Figure 6E, F). Thus, derivatives of the G-baToN system allow for
190 additional degrees of resolution of complex cell-cell interactions.
191
192 **Labeling with HaloTag-conjugated fluorophores enhances sensitivity and signal persistence**
193 We next extended our labeling system further by generating sender cells expressing the
194 HaloTag protein fused to sGFP (sHalo-GFP; Figure 7A)(Los et al., 2008). Covalent attachment
195 of a synthetic fluorophore to sHalo-GFP enabled specific loading onto sender cells (Figure 7B).
196 Co-culture of Alexa Fluor 660 (AF660)-loaded sHalo-GFP sender cells with αGFP receiver cells
197 enabled co-transfer of both GFP and AF660 (Figure 7C). Compared to GFP, transfer of the
198 chemical fluorophore using sHalo-GFP-based labeling of receiver cells led to increased signal-
199 to-noise ratio and higher sensitivity (Figure 7C, D). Importantly, changing from a protein (GFP)
200 to a chemical fluorophore also extended the half-life of labeling, thus enabling partially tunable
201 persistence of labeling after touching (Figure 7E).
202 Next, we coupled the enhanced properties of chemical fluorophore-based labeling with
203 the generalizability of the GCN4-baToN system to assemble a robust and versatile system to
204 label receiver cells that have interacted with two or more different sender cell types (Figure 7F).
205 Co-culturing αGCN4 receiver cells with AF488- and AF660-loaded sGCN4-Halo sender cells
206 generated a spectrum of receiver cells with varying degrees of AF488 and AF660 labeling
207 (Figure 7G). Importantly, the ratio of AF488 to AF660 transferred to the dually labeled receiver
208 cells strongly correlated with the ratio of the two sGCN4-Halo sender populations within the co-

culture, suggesting that this system can quantitively measure higher-order cell-cell interactions (Figure 7H).

**The G-baToN system can function as a vehicle for molecular cargo**

Given the high efficiency of protein transfer using the G-baToN system, we investigated whether cargo molecules could be co-transferred with GFP from sender cells to receiver cells. In addition to the co-transfer of Halo-Tag with sGFP, we also generated sender cells with surface expression of a GFP-tdTomato fusion protein (sGFP-Tom) and uncovered stoichiometric tdTomato and GFP transfer to αGFP receiver cells (Figure 8A, B). Beyond fluorescent labels, we tested whether other cargo could be transferred to receiver cells. We generated sGFP-PuroR-expressing sender cells and found that co-culture of sGFP-PuroR sender cells with αGFP receiver cells led to moderate puromycin resistance of touched receiver cells (Figure 8C, D). Finally, loading of sGCN4-HaloTag sender cells with HaloTag-conjugated, AF647-coupled ssDNA prior to co-culture with αGCN4 receiver cells revealed successful co-transfer of fluorescently labeled ssDNA to receiver cells (Figure 8 E-G). Thus, baToN systems enable contact-dependent transport of different macromolecules between cells.

**DISCUSSION**

Here we developed and optimized a novel cell-cell interaction reporter system and showed that this G-baToN system can record diverse cancer cell-stromal cell interactions in a specific and sensitive manner. Our data document the ability of diverse primary cell types to serve as both sender and receiver cells, suggesting that the G-baToN system is not only simple, sensitive and rapid, but also generalizable. Multicolor derivatives of G-baToN enable qualitative

232 and quantitative analyses of higher-order interactions involving more than two cell types.
233 Finally, the ability to co-transfer protein, DNA and chemical cargo suggests that this platform
234 could be leveraged to manipulate target cell function.

235 Cancer cell-stromal cell interactions can be relatively stable (such as cancer cell
236 interactions with other cancer cells and stromal cells) or transient (such as cancer cell-immune
237 cell interactions and circulating tumor cell (CTC) interactions with endothelial cells during
238 metastasis). The G-baToN system labels receiver cells through transfer of cell surface GFP
239 which, due to its lability, ensures only transient labeling. This is similar to other cell-cell
240 interaction labeling systems (Supplementary Figure 5). Transient labeling is sufficient to label
241 stable cancer cell-stromal cell interactions and many other diverse cell-cell interactions when
242 sender cells consistently express GFP (Figure 1F). This transient labeling should allow dynamic
243 interactions to be detected, ensuring that the labelled receiver cells either are in contact with, or
244 have recently interacted with sender cells.

245 Further optimization of the G-baToN systems could allow shorter or longer term labeling
246 within different biological systems. For example, a G-baToN system where sGFP is inducible
247 may allow physical interactions between cancer cells and stromal cells to be captured with even
248 more precise temporal control. Conversely, we have shown that using chemical fluorophores
249 significantly extends label persistence within receiver cells (Figure 7E), which can be used for
250 longer term labeling of receiver cells that undergo dynamic interactions. Future development of
251 systems that allow for stable receiver cell labeling (perhaps through genetic modification of
252 receiver cells), will facilitate the study of cell-cell interaction induced cell fate determination via
253 contact-dependent linage tracing.

254 As with other cell-cell interaction reporter systems, the G-baToN system relies on cell
255 surface ligand-receptor recognition (Supplementary Table 1-2). While LIPSTIC-based labeling is
256 driven by endogenous ligand-receptor interactions, SynNotch and G-baToN systems rely on
257 exogenous ligand-receptor pairs (Morsut et al., 2016; Pasqual et al., 2018). Consequently, these
258 systems could stabilize normal cell-cell interactions. It is possible that tuning the affinity or
259 expression level of the nanobody could minimize this effect. Inducible G-baToN systems may
260 circumvent these issues, thus ensuring the recording of only *bona fide* interactions. Given that G-
261 baToN-based cell-cell interaction reporter systems can be used as a discovery approach, the
262 consequences of these interactions can be validated by orthogonal methods in the absence of
263 exogenous ligand-receptor pairs.

264 An interesting advantage of the G-baToN system is its ability to mediate cargo transfer.
265 We demonstrated the feasibility of transferring small molecules (HaloTag ligand, Figure 7),
266 functional proteins (puromycin resistant protein, Figure 8C-D), and non-protein macromolecules
267 (ssDNA, Figure 8E-G). Transferred cargo proteins may be able to modify receiver cell signaling
268 or promote cell death. In the future, additional design features could allow cancer cell-stromal
269 cell interaction dependent drug delivery, cell-cell interaction facilitated sgRNA transfer between
270 interacting cells, and digital recording of cell-cell interaction via DNA-barcode transfer. Thus,
271 we expect the G-baToN system to facilitate an even wider array of discoveries about cell-cell
272 interactions in cancer, across other physiological or pathological processes, and within different
273 model organisms.

274 The simplicity of this two-component system, combined with its generalizability across
275 cell types, excellent foreground to background, and rapid labeling, should enable facile analysis
276 of the dynamics of cellular interaction. These types of approaches have the potential to have a

277 broad impact on our ability to understand the outputs of cell-cell interactions in cancer and
278 various other biological systems.
279
280
281 **Figure Legends**
282
283 **Figure 1. GFP-based Touching Nexus (G-baToN) leads to cell-cell interaction-dependent**
284 **receiver cell labeling.**
285 **a.** Schematic of the G-baToN system. Surface GFP (sGFP) on a sender cell is transferred to a
286 receiver cell expressing a cell surface anti-GFP nanobody (αGFP) leading to GFP labeling of the
287 "touched" receiver.
288 **b.** GFP transfer from sGFP-expressing KPT lung cancer sender cells (marked by intracellular
289 tdTomato) to αGFP-expressing 293 receiver cells. Receiver cell labeling is sGFP- and αGFP-
290 dependent. Control sender cells do not express sGFP. Control receiver cells do not express
291 αGFP. Cytoplasmic GFP (Cyto-GFP) is not transferred to receiver cells. Sender and receiver
292 cells were seeded at a 1:1 ratio and co-cultured for 24 hours. Receivers were defined as
293 $Tomato^{neg}PI^{neg}$ cells.
294 **c.** GFP transfer to 293 receiver cells requires direct cell-cell contact. Receiver cells separated
295 from sender cells by a transwell chamber are not labeled. Sender and receiver cells were seeded
296 in upper and lower chambers respectively at a 1:1 ratio and cultured for 24 hours. Receivers were
297 defined as $Tomato^{neg}PI^{neg}$ cells.
298 **d.** GFP transfer to 293 receiver cells requires sGFP-αGFP interaction and is blocked by anti-GFP
299 antibody in a dose-dependent manner. sGFP sender cells were pre-incubated with the indicated

300 concentration of anti-GFP antibody for 2 hours, washed with PBS, and then co-cultured with
301 receiver cells at a 1:1 ratio for 24 hours. Receivers were defined as $Tomato^{neg}PI^{neg}$ cells.
302 **e.** Time-lapse imaging of GFP transfer from a sGFP-expressing sender cell to an αGFP-
303 expressing receiver cell. Time after contact is indicated. Receiver cell is outlined with white
304 dashed line. Scale bar: 10 μm.
305 **f.** Analysis of GFP Mean Fluorescence Intensity (MFI) of αGFP receiver cells (marked by
306 intracellular BFP) co-cultured with sGFP sender cells (marked by intracellular tdTomato) co-
307 cultured for the indicated amount of time. Sender and receiver cells were seeded at a 1:1 ratio.
308 Receivers were defined as $Tomato^{neg}PI^{neg}BFP^{pos}$ cells.
309 **g.** Percentage of labeled αGFP receiver cells after co-culture with different numbers of sender
310 cells for 24 hours. Receivers were defined as $Tomato^{neg}PI^{neg}BFP^{pos}$ cells.
311 **h.** Detection of rare labeled αGFP receiver cells after co-culture with sGFP sender cells at
312 approximately a $1:10^5$ ratio for 24 hours. Receivers were defined as $Tomato^{neg}PI^{neg}BFP^{pos}$ cells.
313
314 **Figure 2. Transmembrane domains and the nanobody affinity impact sGFP transfer and**
315 **receiver cell labeling.**
316 **a.** Schematic of the sender and receiver cells used to determine the impact of different αGFP
317 transmembrane (TM) domains. TM domains contain the TM domain itself as well as membrane
318 proximal regions from the indicated mouse (m) and human (h) proteins.
319 **b.** Different TM domains impact cell surface αGFP expression on 293 receiver cells. Membrane
320 αGFP was accessed by anti-Myc staining. Control receiver cells do not express any nanobody.
321 Mean +/- SD of Myc MFI in triplicate cultures is shown.

322 **c.** VEGFR2 TM domain on αGFP receivers enables highest GFP transfer efficiency. Receiver
323 cells expressing αGFP linked by different TM domains were co-cultured with sGFP sender cells
324 at a 1:1 ratio for 6 hours. Receivers were defined as $Tomato^{neg}PI^{neg}$ cells.
325 **d**. Schematic of the sender and receiver cells used to determine the impact of different αGFP
326 nanobodies on G-baToN-based labeling.
327 **e.** Different nanobodies exhibit different levels of expression on 293 receiver cells. Total αGFP
328 expression was assessed by BFP intensity. Mean +/- SD of GFP MFI in triplicate cultures is
329 shown.
330 **f.** αGFP affinity influences transfer of GFP to touched 293 receiver cells. Receiver cells
331 expressing different αGFP nanobodies were co-cultured with sGFP sender cells at a 1:1 ratio for
332 6 hours. GFP transfer was assessed by flow cytometry. GFP intensity on $Tomato^{neg}PI^{neg}BFP^{pos}$
333 receiver cells is shown as mean +/- SD of triplicate cultures.
334 **g**. Schematic of the sender and receiver cells used to determine the impact of different sGFP TM
335 domains on G-baToN-based labeling. TM domains contain the TM domain itself as well as
336 membrane proximal regions from the indicated mouse (m) and human (h) proteins.
337 **h.** Different TM domains on sGFP impact its expression in 293 sender cells. sGFP expression in
338 sender cells was assessed by flow cytometry for GFP. Mean +/- SD of GFP MFI in triplicate
339 cultures is shown.
340 **i.** PDGFR TM domain on sGFP minimized retrograde transfer of αGFP from receiver cells to
341 293 sGFP sender cells. αGFP transfer to sGFP senders were determined as the percentage of
342 $mCherry^{pos}GFP^{pos}$ sender cells that were also $BFP^{pos}$. Cells were co-cultured for 6 hours at a 1:1
343 ratio. Mean +/- SD of triplicate cultures is shown.
344

345 **Figure 3. G-baToN can be used for touching-based labeling between cancer cells and**
346 **endothelial cells.**
347 **a, b.** G-baToN can detect cancer cell-endothelial cell (EC) interactions. HUVECs expressing
348 αGFP were co-cultured with or without Tomato$^{pos}$ sGFP-expressing lung cancer sender cells at a
349 1:1 ratio for 24 hours. (a) Representative images of Tomato$^{pos}$ sGFP-expressing lung cancer
350 sender cells co-cultured with either control HUVEC receiver cells (HUVECs expressing BFP) or
351 αGFP HUVEC receiver cells at a 1:1 ratio for 24 hours . Scale bars = 50 μm. (b) MFI of GFP on
352 PI$^{neg}$Tomato$^{neg}$BFP$^{pos}$CD31$^{pos}$ Receiver cells was assessed by flow cytometry and is shown as
353 mean +/- SD of triplicate cultures. ** $p<0.01$, n=3.
354 **c,d.** G-baToN can detect endothelial cell (EC)-smooth muscle cell (SMC) interactions. Primary
355 human umbilical artery smooth muscle cells (HUASMC) expressing αGFP were co-cultured
356 with or without sGFP-expressing HUVEC senders at a 1:1 ratio for 24 hours. (c) Representative
357 images of sGFP-expressing HUVEC sender cells co-cultured with either control HUASMC
358 receiver cells (expressing BFP) or αGFP HUASMC receiver cells at a 1:1 ratio for 24 hours.
359 Scale bars = 50 μm. (d) MFI of GFP on PI$^{neg}$BFP$^{pos}$ receiver cells was assessed by flow
360 cytometry and is shown as mean +/- SD of triplicate cultures. ** $p<0.01$, n=3.
361 **e,f,g**. G-baToN can detect cancer cell-endothelial cell (EC) interactions in 3D-microfluidic
362 culture. (e) Details on design of 3D-microfluidic devices for cancer cell-endothelial cell co-
363 culture. (f) Representative images of Tomato$^{pos}$ sGFP-expressing lung cancer sender cells co-
364 cultured with either control HUVEC receiver cells (HUVECs expressing BFP) or αGFP HUVEC
365 receiver cells at a 1:10 ratio for 24 hours . Scale bars = 200 μm. (g) Average number of GFP$^{pos}$
366 HUVEC after co-culture with cancer cells for 24 h. 10 areas from three chips with 200X
367 magnification were used for the quantification. ** $p<0.01$, n = 10.

368

369 **Figure 4. G-baToN can detect T cells-cancer cells interactions.**

370 **a,b,c.** G-baToN can detect cancer cell-T cell interactions in vitro. (a) Primary human $CD4^{pos}$ or

371 $CD8^{pos}$ T cells were co-cultured with sGFP-expressing lung cancer sender cells (A549 cells) at a

372 2:1 ratio for 24 hours. Representative image of A549 cell and CD4 T cell interactions. Scale bars

373 = 10 μm.(b,c) A549 cells expressing sGFP can transfer GFP to αGFP primary human $CD4^{pos}$ (b)

374 or $CD8^{pos}$ (c) T cells after co-culture at a 1:1 ratio for 24 hours. Receivers were defined as Near-

375 $IR^{neg}BFP^{pos}CD4^{pos}/CD8^{pos}$ T cells.

376 **d,e.** G-baToN can detect cancer cell-T cell interactions in vivo. (d) Experiment design for cancer

377 cell-T cell interactions in vivo. $1X10^6$ sGFP-expressing lung cancer sender cells were

378 transplanted into NSG mice at day 0. $4X10^6$ αGFP primary human $CD4^{pos}$ T cell were

379 transplanted into tumor-bearing mice at day 21. 1 day after T cell transplantation (day 22), T

380 cells in mouse lung were analyzed via FACS. (e) sGFP-expressing cancer cell can transfer

381 GFP to αGFP-expressing primary human $CD4^{pos}$ T cells. Receives were defined as

382 $PI^{neg}BFP^{pos}CD4^{pos}$T cells.

383

384 **Figure 5. G-baToN can detect neuron-cancer cell, neuron-astrocyte interactions.**

385 **a.** Representative image of sGFP-expressing cancer sender cells co-cultured with either control

386 neuron receivers or αGFP neuron receivers at a 1:1 ratio for 24 hours. Neurons were stained with

387 Microtubule Associated Protein 2 (Map2). Scale bars = 50 μm.

388 **b.** Quantification of supplementary Figure 5a using images from 10 different fields. Each dot

389 represents a field. The bar indicates the mean +/- SD. $GFP^{pos}$ neurons were defined as

390 $Map2^{pos}Tomato^{neg}$ cells with GFP. ** $p<0.01$, n=10.

391 **c.** Representative images of sGFP-expressing astrocyte sender cells co-cultured with either
392 control neuron receivers or αGFP neuron receivers at a 1:2 ratio for 24 hours. Neurons were
393 stained with Map2. Scale bars = 50 μm. Higher magnification of the boxed areas are shown on
394 the right.
395 **d.** Quantification of Figure 5c using images from 10 different fields. Each dot represents a field.
396 The bar indicates the mean +/- SD. $GFP^{pos}$ neurons were defined as $Map2^{pos}$ cells with GFP. **
397 $p<0.01$, n=10.
398
399 **Figure 6. Multicolor-baToN systems enable recording of higher order interactions.**
400 **a.** Diagram of the Reciprocal-baToN system. Cell A expresses sGFP and αmCherry (tagged by
401 intracellular BFP), Cell B expresses smCherry and αGFP (tagged by Myc-tag).
402 **b.** Representative FACS plots of cell A and cell B monocultures (left 2 panels) and after co-
403 culture at a 5:1 ratio for 24 hours. Percent of labeled cells is indicated as mean +/- SD of
404 triplicate cultures.
405 **c.** Schematic of the AND gate-baToN system. sGFP and smCherry sender cells express either
406 sGFP or mCherry. Dual receiver cells express both αGFP (LaG17, tagged by Myc-tag) and
407 αmCherry (LaM4, tagged by intracellular BFP).
408 **d.** Representative FACS plots of dual receiver 293 cells cultured with the indicated 293 sender
409 cells at 1:1 (for single sender cell) or 1:1:1 (for dual sender cells) ratios. Percent of labeled
410 receiver cells (gated as $BFP^{pos}$) after 24 hours of co-culture is indicated as mean +/- SD of
411 triplicate cultures.

412 **e**. Diagram of the BFP/GFP AND gate-baToN system. sBFP sender cells express intracellular
413 Tomato and surface BFP, sGFP sender cells express intracellular Tomato and surface GFP.
414 Common receiver cells expressed αGFP.
415 **f.** Representative FACS plots of common receiver 293 cells cultured with the indicated
416 $Tomato^{pos}$ sender cells at 1:1 (for single sender cell) or 1:1:1 (for dual sender cells) ratios.
417 Receiver cells were gated as $Tomato^{neg}PI^{neg}$. Percent of labeled common receiver cells after 24
418 hours of co-culture is indicated as mean +/- SD of triplicate cultures.
419
420 **Figure 7. The HaloTag-baToN system enable quantitative and sensitive cell-cell**
421 **interaction-dependent receiver cell labeling.**
422 **a.** Diagram of HaloTag-baToN system. Sender cells (marked by intracellular 2A-mCherry)
423 express surface HaloTag-GFP fusion which can be loaded with HaloTag ligands (in this example
424 AF660). Receiver cells express αGFP (LaG17, tagged by intracellular BFP).
425 **b.** Labeling HaloTag-expressing sender cells with AF660 fluorophore. Representative FACS
426 plots of KP (lung adenocarcinoma) sender cells expressing either sGFP or sGFP-sHaloTag
427 incubated with AF660-conjugated HaloTag ligand for 5 minutes on ice. AF660 specifically
428 labeled sHaloTag-GFP sender cells but not sGFP sender cells.
429 **c.** Representative plot of GFP and AF660 intensity in αGFP 293 receiver cells co-cultured with
430 HaloTag-GFP KP (lung adenocarcinoma) sender cells at a 1:1 ratio for 6 hours. Receivers were
431 defined as $mCherry^{neg}PI^{neg}BFP^{pos}$ cells.
432 **d.** AF660 transfer to αGFP 293 receiver cell is rapid after cell-cell interaction. AF660 MFI shift
433 was detected after mixing sHalo-GFP senders and αGFP receivers and co-culture for 10 minutes.

434 AF660 MFI shift was more dramatic than GFP. Receivers were defined as
435 mCherry$^{neg}$PI$^{neg}$BFP$^{pos}$ cells.
436 **e.** Slower AF660 quenching in touched receiver cells after removing sHalo-GFP senders. After 6
437 hours co-culture, GFP/AF660 positive receiver cells were purified via FACS. Analysis of
438 GFP/AF660 MFI in purified receiver cells showed rapid GFP degradation but slower AF660
439 quenching. Receivers were defined as mCherry$^{neg}$PI$^{neg}$BFP$^{pos}$ cells.
440 **f.** Diagram of dual color GCN4-HaloTag-baToN system. Sender cells (marked by intracellular
441 2A-mCherry) express surface 4XGCN4 associated with HaloTag, loaded with either AF488- or
442 AF660- conjugated HaloTag ligand. Receiver cells express αGCN4 (tagged by intracellular
443 BFP).
444 **g.** Representative FACS plots of αGCN4 receiver cells co-cultured with the indicated sender
445 cells at 1:1 (for single sender cell) or 1:1:1 (for dual sender cells) ratios. Percent of labeled
446 receiver cells (gated as mCherry$^{neg}$PI$^{neg}$BFP$^{pos}$) after 6 hours of co-culture is indicated as mean
447 +/- SD of triplicate cultures.
448 **h.** AF488/AF660 GCN4-HaloTag sender ratio in the co-culture directly proportional to
449 AF488/AF660 intensity (MFI) of αGCN4 receiver after 6 hours of co-culture. Receivers were
450 defined as mCherry$^{neg}$PI$^{neg}$BFP$^{pos}$ cells.
451
452 **Figure 8. The G-baToN system can co-transfer cargo molecules into touched receiver cells.**
453 **a.** Diagram of surface tdTomato-GFP (sGFP-Tom) co-transfer into touched receiver cells.
454 Sender cell expresses sGFP-tdTomato and receiver cell expresses αGFP (tagged by intracellular
455 BFP).

456 **b.** Representative FACS plots of αGFP 293 receiver cells cultured with the indicated sender cells
457 at 1:1 ratio for 24 hours. Percent of GFP/Tomato dual labeled receiver cells is indicated as mean
458 +/- SD of $BFP^{pos}$ cells from triplicate cultures.
459 **c.** Diagram of GFP-PuroR co-transfer system. Sender cell expresses surface GFP associated with
460 PuroR (marked by intracellular tdTomato), receiver cell expresses αGFP (tagged by intracellular
461 BFP). PuroR: Gcn5-related N-acetyltransferase.
462 **d.** Co-transfer of GFP-PuroR from sGFP-PuroR sender cells to αGFP 293 receiver cells confers
463 puromycin resistance to receiver cells. Control, sGFP or sGFP-PuroR sender cells were co-
464 cultured with αGFP 293 receiver cells for 24 hours at a 4:1 ratio before treatment with
465 different dose of puromycin for 48 hours. $tdTomato^{neg}PI^{neg}BFP^{pos}$ cell numbers were counted via
466 FACS.
467 **e.** Diagram of using GCN4-HaloTag sender to transfer ssDNA into αGCN4 receiver cells.
468 Sender cells (marked by intracellular 2A-mCherry) express surface 4XGCN4 associated with
469 HaloTag, loaded with 5' HaloTag ligand, 3' biotin dual conjugated ssDNA (21 nt), then stained
470 with Avidin-AF647. Receiver cells express αGCN4 (tagged by intracellular BFP).
471 **f.** Loading of sender cells with ssDNA. Representative FACS plots of 293 sender cells
472 expressing either sGCN4 or sGCN4-Halo were loaded with 5' HaloTag-ligand, 3' biotin dual
473 conjugated ssDNA (21nt), then stained with Avidin-AF647. AF647 specifically labeled loaded
474 sGCN4-Halo sender cells but not sGCN4 sender cells.
475 **g.** Representative plot of AF647 intensity in αGCN4 293 receiver cells co-cultured with GCN4-
476 HaloTag 293 sender cells at a 1:1 ratio for 6 hours. Receivers were defined as
477 $mCherry^{neg}PI^{neg}BFP^{pos}$ cells.
478

479 **Supplementary Figure 1. GFP transfer requires direct GFP-αGFP interaction.**

480 **a.** GFP protein is transferred to receiver cells. Western blot analysis of FACS purified Control
481 and αGFP receiver 293 cells cultured in isolation or co-culture with sGFP Tomato-positive
482 sender cells (mouse KPT lung cancer cells) for 24 hours. sGFP but not Tomato is present in
483 touched αGFP receiver cells. Human mitochondrial antigen (hu-Mito) is a marker for receiver
484 cells. GAPDH shows loading. Rightmost lane is sGFP sender cells.

485 **b.** GFP cannot be transferred from fixed sGFP sender cells to live αGFP receiver cells. sGFP
486 sender cells were fixed in 1% PFA for 5 minutes and washed with PBS before co-cultured with
487 αGFP receiver cells at a 1:1 ratio for 24 hours. Receivers were defined as $Tomato^{neg}PI^{neg}BFP^{pos}$
488 cells.

489 **c.** GFP transfer to 293 receiver cells required sGFP-αGFP recognition. GFP is transferred from
490 sGFP sender cells to αGFP-receiver cells but not from sGFP sender cells to αmCherry-receiver
491 cells. Control receiver cells do not express any nanobody. Sender and receiver cells were co-
492 cultured at a 1:1 ratio for 24 hours. Receivers were defined as $Tomato^{neg}PI^{neg}BFP^{pos}$ cells.

493 **d.** GFP transfer to receiver cells is accompanied by a reduction of GFP on the sender cells. GFP
494 expression on sender cells after 24 hour co-culture with control or αGFP-expressing 293 receiver
495 cells at a 1:1 ratio. Co-culture with αGFP expressing but not control receiver cells reduced GFP
496 on sGFP sender cells. Senders were defined as $Tomato^{pos}DAPI^{neg}BFP^{neg}$ cells.

497 **e.** GFP transfer is accompanied with αGFP internalization on receiver cells. Analysis of surface
498 αGFP (Myc-tag) on 293 receiver cell co-cultured for 24 hours with sGFP sender cells. Receivers
499 were defined as $Tomato^{neg}PI^{neg}$ cells.

500 **f.** GFP transfer to 293 receiver cells is partially dependent on membrane dynamics of
501 endocytosis. Both a clathrin inhibitor (Pitstop, 20 μM) and a dynamin inhibitor (Dyngo 4a, 10

502 μM) partially inhibit GFP transfer from sGFP sender cells to αGFP receivers. Inhibitors were
503 present during the 24 hour co-culture. Receivers were defined as Tomato$^{neg}$PI$^{neg}$ cells.
504 **g.** GFP transfer to αGFP 293 receiver cells can be very rapid. A shift in GFP MFI was detected 5
505 minutes after mixing sGFP sender cells with αGFP receiver cell. Receivers were defined as
506 Tomato$^{neg}$PI$^{neg}$BFP$^{pos}$ cells. MFI mean +/- SD of triplicate cultures is shown.
507 **h.** Rapid GFP degradation in touched receiver cells after removal of the sGFP sender cells. After
508 6 hours co-culture, GFP positive receiver cells were purified by FACS followed by culture
509 without sender cells. Receivers were defined as mCherry$^{neg}$PI$^{neg}$BFP$^{pos}$ cells. GFP MFI in
510 receiver cells reduced rapidly ($T_{1/2}$ approximately 2 hours). MFI mean +/- SD of triplicate
511 cultures is shown.
512
513 **Supplementary Figure 2. G-baToN is a generalized system that can be used for touching-**
514 **based labeling between various cell types.**
515 **a.** Many different cell lines and primary cell types can serve as receiver cells. Receiver cells
516 expressing αGFP were co-cultured with sGFP-expressing KPT sender cells for 24 hours. MFI of
517 GFP on Tomato$^{neg}$PI$^{neg}$BFP$^{pos}$ receiver cells was assessed by FACS analysis and is shown as fold
518 change relative to monocultured receiver cells. For lung epithelial cells and kidney epithelial
519 cells MFI of GFP on Tomato$^{neg}$PI$^{neg}$BFP$^{pos}$EpCAM$^{pos}$ cells are shown as mean +/- SD of
520 triplicate cultures. SkMC: skeletal muscle cells. Astro: Astocytes. Hepato: hepatocytes. Spleno:
521 splenocytes.
522 **b.** Many different cell lines and primary cell types can serve as sender cells. Sender cells
523 expressing sGFP were co-cultured with αGFP 293 receiver cells for 24 hours. MFI of GFP on
524 mCherry$^{neg}$PI$^{neg}$BFP$^{pos}$ receiver cells was assessed by FACS and is shown as fold change

525 relative to monocultured 293 receiver cells. Mean +/- SD of triplicate cultures is shown.

526 **c,d,e,f.** Diverse primary mouse cells expressing sGFP can transfer GFP to αGFP 293 receivers.

527 Different primary sender cells were first sorted based on their cell surface markers, then

528 transduced with lentiviral vectors expressing sGFP before being co-cultured with αGFP 293

529 receiver cells for 24 hours. Percentage of $mCherry^{neg}PI^{neg}BFP^{pos}GFP^{pos}$ receiver cells was

530 assessed by flow cytometry. For each primary sender, approximate $sGFP^{pos}$ sender : $\alpha GFP^{pos}$

531 receiver ratio is indicated: c. Lung epithelial cells (1:180) (sorted $EpCam^{pos}$ cells from

532 dissociated adult lung); d. Kidney epithelial cells (1:20) (sorted $EpCam^{pos}$ cells from dissociated

533 adult kidney); e. Splenocyte (1:20); f. Cardiomyocyte (1:5) (sorted $Sirpa^{pos}$ cells from dissociated

534 adult heart). Percent of labeled cells is indicated as mean +/- SD of triplicate cultures.

535

536 **Supplementary Figure 3. X-baToN systems enable fluorescent labeling via various antigen-**

537 **nanobody/scFV pairs.**

538 **a.** Schematic of the surface BFP (sBFP)-baToN system. Sender cell (marked by intracellular

539 tdTomato) expresses sBFP and receiver cell expresses αGFP.

540 **b.** The cross reactivity of αGFP with BFP allow BFP to be transferred from sBFP sender to

541 αGFP receiver cells. sBFP senders and αGFP receivers were co-cultured at 1:1 ratio for 24 hours.

542 Receivers were defined as $toTomato^{neg}PI^{neg}$ cells. BFP MFI of receiver cells is shown as mean

543 +/- SD of triplicate cultures.

544 **c.** Schematic of the surface mCherry (smCherry)-baToN system. Sender cell (marked by

545 intracellular GFP) expresses smCherry and receiver cell expresses αmCherry (tagged by

546 intracellular BFP)

547 **d.** The pairing between mCherry and αmCherry enable mCherry transfer from smCherry 293
548 sender cells to αmCherry-expressing 293 receiver cells. smCherry senders are not able to transfer
549 mCherry to αGFP receiver cells. smCherry sender cells were co-cultured with αGFP or
550 αmCherry receiver cells at a 1:1 ratio for 24 hours. Receivers were defined as $GFP^{neg}BFP^{pos}$
551 cells. mCherry MFI of receiver cell is shown as mean +/- SD of triplicate cultures. smCherry 293
552 sender is not able to transfer mCherry to αGFP 293 receiver.
553 **e.** Schematic of the surface GCN4 (sGCN4)-baToN system. Sender cells (marked by intracellular
554 2A-mCherry) express cell surface 4X GCN4 peptide fused with GFP. Receiver cells express a
555 cell surface anti-GCN4 single-chain variable fragment (scFV; αGCN4, tagged by intracellular
556 BFP).
557 **f.** The pairing between GCN4 and αGCN4 enables co-transfer of GFP from 4X sGCN4-GFP
558 senders to αGCN4 receivers 24 hours after co-culture at a 1:1 ratio. Receivers were defined as
559 $mCherry^{neg}PI^{neg}BFP^{pos}$ cells. GFP MFI of receiver cell is shown as mean +/- SD of triplicate
560 cultures. sGFP sender are not able to transfer GFP to αGCN4 receivers.
561
562 **Supplementary Figure 4. Dual color-baToN systems enable labeling in complex cell-cell**
563 **interaction systems.**
564 **a.** Representative image of reciprocal labeling of cell A and cell B co-cultured for 24 hours. Cells
565 are outlined with a white dashed line. Cell A is BFP and GFP double positive and Cell B is
566 mCherry positive. Touched cell A is BFP, GFP and mCherry triple positive and touched cell B is
567 GFP and mCherry double positive (pointed out by white letter). Scale bar: 10 μm.

568 **b.** Representative image of dual receiver cells co-cultured with indicated sender cells. Cells are
569 outlined with a white dashed line. Dual receiver cells are BFP positive and sender touched dual
570 receiver cells are pointed out by white arrows. Scale bar: 10 μm.
571
572 **Supplementary Figure 5. Features of the SynNotch, LIPSTIC, and G-BaToN cell-cell**
573 **interaction reporter systems.**
574 Overview of systems that enable labeling of cells after cell-cell contact.
575
576 **ACKNOWLEDGEMENTS**
577 We thank the Stanford Shared FACS and Cell Sciences Imaging Facilities for technical
578 support; A. Orantes for administrative support, N. Kipniss and Y.T. Shue for critical reagents; D.
579 Feldser, J. Sage, Y. Chien, N. Kipniss and members of the Winslow laboratory for helpful
580 comments. R.T. was supported by a Stanford University School of Medicine Dean's Postdoctoral
581 Fellowship and a TRDRP Postdoctoral fellowship (27FT-0044). C.W.M. was supported by the
582 NSF Graduate Research Fellowship Program and an Anne T. and Robert M. Bass Stanford
583 Graduate Fellowship. W.L. was supported by a NCI Career Development Award (NIH K25-
584 CA201545). This work was supported by NIH R01-CA175336 (to M.M.W), NIH R01-
585 CA207133 (to M.M.W) and NIH R01-CA230919 (to M.M.W) and in part by the Stanford
586 Cancer Institute support grant (NIH P30-CA124435), 1S10OD01227601 from the National
587 Center for Research Resources (NCRR) and S10RR027431-01 from National Institutes of Health
588 (NIH).
589
590 **METHODS**

591 *Cells, Plasmids and Reagents:*

592 HEK-293T, B16-F10, A549, H460 and HUVEC cells were originally purchased from ATCC;
593 HUASMC were purchased from PromoCell (C-12500); H82 cells were kindly provided by Julien
594 Sage (Stanford School of Medicine); KP (238N1) and KPT (2985T2) lung adenocarcinoma cells
595 were generated in the Winslow Lab. HEK-293T, 238N1, 2985T2 and B16-F10 cells were
596 cultured in DMEM containing 10% FBS, 100 units/mL penicillin and 100 μg/mL streptomycin.
597 A549, H460 and H82 cells were cultured in RPMI1640 media containing 10% FBS, 100
598 units/mL penicillin and 100 μg/mL streptomycin. HUVECs were cultured in Vascular Cell Basal
599 Medium (ATCC, PCS-100-030) with Endothelial Cell Growth Kit (ATCC, PCS-100-041);
600 HUASMC were cultured in Smooth Muscle Cell Growth Medium 2 (PromoCell, C-22062). All
601 cell lines were confirmed to be mycoplasma negative (MycoAlert Detection Kit, Lonza).
602 Pitstop (ab120687) and Dyngo 4a (ab120689) were purchased from Abcam.
603 All plasmids used in this study are listed in Supplementary Table 1 and will be available on
604 Addgene.
605

606 *Antibodies:*

607 Anti-GFP antibody was purchased from MyBioSource (MBS560494), anti-RFP antibody was
608 purchased from Rockland (600-401-379), anti-human mitochondria antibody was purchased
609 from Abcam (ab92824), anti-GAPDH antibody was purchased from Cell Signaling Technology
610 (5174S)
611

612 *Lentiviral Vector Packaging:*

613 Lentiviral vectors were produced using polyethylenimine (PEI)-based transfection of 293T cells
614 with the plasmids indicated in Supplementary Table 1, along with delta8.2 and VSV-G
615 packaging plasmids in 150-mm cell culture plates. Sodium butyrate (Sigma Aldrich, B5887) was
616 added 8 hours after transfection to achieve a final concentration of 20 mM. Medium was
617 refreshed 24 hours after transfection. 20 mL of virus-containing supernatant was collected 36,
618 48, and 60 hours after transfection. The three collections were then pooled and concentrated by
619 ultracentrifugation (25,000 rpm for 1.5 hours), resuspended overnight in 100 µL PBS, then
620 frozen at -80°C.
621
622 *Generation of Stable Cell Lines*
623 Parental cells were seeded at 50% confluency in a 6-well plate the day before transduction (day
624 0). The cell culture medium was replaced with 2 mL fresh medium containing 8 µg/mL
625 hexadimethrine bromide (Sigma Aldrich, H9268-5G), 20 µL ViralPlus Transduction Enhancer
626 (Applied Biological Materials Inc., G698) and 40 µL concentrated lentivirus and cultured
627 overnight (Day 1). The medium was then replaced with complete medium and cultured for
628 another 24 hours (Day 2). Cells were transferred into a 100 mm cell culture dish with appropriate
629 amounts of puromycin (Dose used: 293T: 2 µg/mL; 238N1: 3 µg/mL; 2985T2: 2 µg/mL) and
630 selected for 48 hours (Day 3). After selection, FACS analysis was performed using fluorescent
631 markers indicated in Supplementary Table 2 for validation of selection efficiency.
632
633 *Transwell Co-culture Assay*
634 The Corning® Transwell® polycarbonate membrane cell culture inserts were purchased from
635 Corning Inc (3422 : CS, Corning, NY). sGFP sender cells were seeded in the upper chamber

636 inserts of the transwell ($1\times10^5$/insert). The inserts were then placed back into the plate pre-
637 seeded with $1\times10^5$/well αGFP receiver cells and cultured in a humidified incubator at 37 °C,
638 with 5% $CO_2$ for 24 hours. sGFP sender and αGFP receiver cells co-cultured in the same plate
639 under the same conditions were used as control. After 24 hours, the upper chamber inserts were
640 removed, cells in the lower chamber were trypsinized and analyzed by flow cytometry.
641
642 *Live and Fixed Cell Imaging*
643 For live cell microscopy, $2\times10^4$ sGFP sender and $2\times10^4$ αGFP receiver cells were seeded into
644 35-mm FluoroDish Cell Culture Dishes (World Precision Instruments, FD35-100) and
645 immediately imaged under a DeltaVision OMX (GE Healthcare) microscope with a 60x oil
646 objective lens (Olympus) in a humidified chamber at 37 °C with 5% $CO_2$. One image was taken
647 per minute for three hours. Images were collected with a cooled back-thinned EM-CCD camera
648 (Evolve; Photometrics).
649
650 For fixed cell microscopy, sender and receiver cells were seeded at the ratios indicated in
651 Supplementary Table 2 with a total number of $1\times10^5$ cells onto Neuvitro coated cover slips
652 (Thermo Fisher Scientific, NC0301187) in a 12-well cell culture plate. 24 hours after co-culture,
653 cells were fixed in 4% paraformaldehyde (PFA) PBS solution at room temperature for 10
654 minutes and washed with PBS and distilled water three times each, before mounting onto slides
655 using 50% glycerol. Images were captured using a Leica DMI6000B inverted microscope with
656 an 40x oil objective lens. For quantification, GFP-containing receiver cells were counted.
657 Multiple coverslips were analyzed across independent experiments (n=10).
658

659 *Western Blot*

660 $5\times10^6$ sGFP sender and $5\times10^6$ αGFP receiver cells were co-cultured in a 100mm cell culture dish
661 for 24 hours. Cells were trypsinized, resuspended in FACS buffer containing propidium iodide
662 (PI) (PBS, 2% FBS, 1 mM EDTA, and 1.5 μM PI). tdTomato$^{neg}$PI$^{neg}$ cells were sorted and lysed
663 in RIPA buffer (50 mM Tris-HCl (pH 7.4), 150 mM NaCl, 1% Nonidet P-40, and 0.1% SDS)
664 and incubated at 4 °C with continuous rotation for 30 minutes, followed by centrifugation at
665 12,000 × rcf for 10 minutes. The supernatant was collected, and the protein concentration was
666 determined by BCA assay (Thermo Fisher Scientific, 23250). Protein extracts (20–50 μg) were
667 dissolved in 10% SDS-PAGE and transferred onto PVDF membranes. The membranes were
668 blocked with 5% non-fat milk in TBS with 0.1% Tween 20 (TBST) at room temperature for one
669 hour, followed by incubation with primary antibodies diluted in TBST (1:1000 for anti-GFP,
670 anti-Tomato (RFP) and anti-human mitochondria (hu-Mito), 1:5000 for anti-GAPDH) at 4 °C
671 overnight. After three 10-minutes washes with TBST, the membranes were incubated with the
672 appropriate secondary antibody conjugated to HRP diluted in TBST (1:10000) at room
673 temperature for 1 hour. After three 10-minutes washes with TBST, Protein expression was
674 quantified with enhanced chemiluminescence reagents (Fisher Scientific, PI80196).

675

676 *GFP/AF660 Stability*

677 To assess the stability of GFP and AF660 in touched receiver cells, $1\times10^7$ sGFP or sHalo-GFP
678 sender cells were co-cultured with $1\times10^7$ αGFP receiver cells in a 150mm cell culture dish for 6
679 hours. Cells were then trypsinized and resuspended in FACS buffer containing propidium iodide.
680 mCherry$^{neg}$PI$^{neg}$BFP$^{pos}$ cells were sorted and $1\times10^5$ cells were re-plated in 12-well plate and
681 cultured for 2, 4, 6, 8, 12, 24 and 48 hours in DMEM containing 10% FBS, 100 units/mL

682 penicillin and 100 µg/mL streptomycin. GFP or AF660 intensity was assessed via FACS analysis
683 of mCherry$^{neg}$PI$^{neg}$BFP$^{pos}$ cells and shown as Mean +/- SD of GFP/AF660 MFI in triplicate
684 cultures.
685
686 *Puromycin Resistant Protein Transfer Assay*
687 To validate puromycin resistant protein (GCN5-Related N-Acetyltransferases, PuroR) function
688 in sender cells, $5\times10^6$ HEK-293T cells were transfected with sGFP-PuroR-PDGFR, sGFP-
689 PDGFR or sGFP-PDGFR-IRES-PuroR in a 100-mm cell culture dish for 12 hours before re-
690 plating into a 12-well plate ($1\times10^5$ cells/well). 24 hours after transfection, cells were treated with
691 1, 2 or 5 µg/mL puromycin for 24 hours. To count the number of viable receiver cells co-
692 cultured with sGFP-PuroR sender cells, $2\times10^5$ αGFP receiver cells were co-cultured with $8\times10^5$
693 sGFP or sGFP-PuroR sender cells in a 6-well plate. 24 hours after co-culture, cells were treated
694 with 0, 1, 3 µg/mL puromycin for 48 hours. Viable tdTomato$^{neg}$PI$^{neg}$BFP$^{pos}$ receiver cells were
695 counted via FACS.
696
697 *Primary Mouse Cell Isolation*
698 Mouse (C57BL/6J, The Jackson Laboratory) lung, kidney, heart, hindlimb skeleton muscle,
699 spleen and liver tissue were dissected, cut into small pieces and digested in 5 mL tissue digest
700 media (3.5 mL HBSS-Ca2+ free, 0.5 mL Trypsin-EDTA (0.25%), 5mg Collagenase IV
701 (Worthington), 25 U Dispase (Corning) for 30 minutes in hybridization chamber at 37˚C with
702 rotation. Digestion is then neutralized by adding 5 mL ice cold Quench Solution (4.5 mL L15
703 media, 0.5 mL FBS, 94 µg DNase). Single cell suspensions were generated by filtering through a
704 40uM cell strainer, spinning down at 500 rcf for 5 minutes and washed with PBS twice

705 For primary mouse lung epithelial cells, kidney epithelial cells and cardiomyocyte isolation and
706 culture, the single cell pellets were resuspended in 1mL FACS buffer containing 1:300 dilution
707 of anti-EpCam-AF467 (Biolegend, 118211) (for lung and kidney epithelial cell ) or anti-Sirpa-
708 AF467 (Biolegend, 144027) (for cardiomyocyte) antibody and incubated on ice for 20 minutes
709 before FACS sorting. $DAPI^{neg}EpCam^{pos}$ or $DAPI^{neg}Sirpa^{pos}$ cells were sorted and seeded onto a
710 100 mm culture dish precoated with 5 μg/$cm^2$ Bovine Plasma Fibronectin (ScienCell, 8248).
711 For primary skeleton muscle cell, splenocyte and hepatocyte culture, the single cell pellets were
712 resuspended in DMEM containing 20% FBS, 200 units/mL penicillin and 200 μg/mL
713 streptomycin, amphotericin and cultured in 100-mm culture dish at 37$^{o}$C for 1 hour to remove
714 fibroblast cells. The supernatant containing primary skeletal muscle cells, splenocytes and
715 hepatocytes was then transferred into a new 100-mm culture dish precoated with 5 μg/$cm^2$
716 Bovine Plasma Fibronectin (ScienCell, 8248).
717
718 *Conjugation of HaloTag Ligand to Oligonucleotides*
719 Oligonucleotides to be conjugated with the HaloTag ligand were synthesized with a 5' C12-
720 linked amine and a 3' biotin group (IDT). Oligonucleotides were initially ethanol-precipitated
721 and subsequently resuspended to 1 mM in conjugation buffer (100 mM Na2HPO4 (Sigma-
722 Aldrich S9763), 150 mM NaCl (Thermo Fisher Scientific S271), pH 8.5). Resuspended oligos
723 were combined with an equal volume of the HaloTag ligand succinimidyl ester (O4) (Promega
724 P6751) resuspended in N,N- dimethylformamide (Sigma-Aldrich D4551) with a 30-fold molar
725 excess of the ligand. Conjugation reactions were conducted overnight at room temperature with
726 constant agitation prior to final cleanup via ethanol precipitation.
727

728 *Loading of HaloTag-Expressing Sender Cells*

729 Prior to loading with HaloTag-conjugated elements, sender cells were washed once in cold PBS
730 following detachment and subsequently resuspended in cold Cell Staining Buffer (BioLegend
731 42021). For loading of HaloTag-conjugated fluorophores, senders were stained at a density of
732 1.00E+07 cells/mL on ice for five minutes in the presence of either 1 µM HaloTag-Alexa Fluor
733 488 (Promega G1001) or 3.5 µM HaloTag-Alexa Fluor 660 (Promega G8471). Stained sender
734 cells were then washed twice in Cell Staining Buffer (500 rcf for 5 min at 4˚C) prior to
735 resuspension in growth media in preparation for co-culture.

736 For loading with HaloTag-conjugated oligonucleotides, sender cells were initially resuspended
737 and incubated with 100 µg/mL salmon sperm DNA (Thermo Fisher Scientific 15632011).
738 Sender cells were then incubated with 3.5 µM HaloTag-conjugated oligonucleotides
739 (5AmMC12/TCTAGGCGCCCGGAATTAGAT/3Bio) and subsequently washed once.
740 Oligonucleotide-loaded sender cells were then stained with 5 µg/mL streptavidin-conjugated
741 Alexa Fluor 647 (Thermo Fisher Scientific S32357) for 30 minutes on ice. The loaded, stained
742 senders were then washed twice and resuspended in growth media in preparation for co-culture.

743

744 *3D-microfluidic cancer cell-endothelial cell co-culture*

745 The master mold of microfluidic chips was fabricated using a 3D printer (Titan HD, Kudo3D
746 Inc. Dublin, CA). The surface of the molds was spray-coated with silicone mold release (CRC,
747 cat. No.: 03300) and PDMS (poly-dimethyl siloxane, Sylgard 182, Dow Corning) was poured on
748 it. After heat curing at 65˚C for approximately 5 hours, the solidified PDMS replica was peeled
749 off from the mold. Holes were made at both ends of each channel in the PDMS replica using a
750 biopsy punch. The PDMS replica was then bonded to precleaned microscope glass slides (Fisher

751 Scientific) through plasma treatment (Harrick Plasma PDC-32G, Ithaca, NY). Microfluidic chips
752 were UV-treated overnight for sterilization before cell seeding.
753 A basement membrane extract (BME) hydrogel (Cultrex™ reduced growth factor basement
754 membrane matrix type R1, Trevigen, Cat #: 3433-001-R1) was injected into the middle hydrogel
755 channel of the chips placed on a cold pack and then transferred to rectangular 4-well cell culture
756 plates (Thermo Scientific, Cat #: 267061) followed by incubation at 37˚C in a cell culture
757 incubator for 30 minutes for gelation. After gelation, 10 uL of human umbilical vein endothelial
758 cells(HUVECs) resuspended at the density of ~ $1 \times 10^6$ cells/mL was injected to the blood
759 channel of the chips and endothelial cell growth medium was added to the other side channel.
760 After incubation for 3h for cells to adhere, old medium in both side channels was replaced with
761 fresh medium. The next day, samples were placed on a rocking see-saw shaker (OrganoFlow® L,
762 Mimetas) that generates a pulsatile bidirectional flow to mimic the dynamic native environment
763 and cultured for 4 more days to form a complete endothelium. Cell culture medium was changed
764 every other day. Then, medium in the blood channel of the chips was removed and 10 uL of
765 sGFP-expressing lung adenocarcinoma cell at the density of ~ $1 \times 10^5$ cells/mL was injected and
766 cultured for 24 hours before imaging. Images were captured using an EVOS fl auto imaging
767 system (Life Technologies).
768
769 *Primary Neuron and Astrocyte Cultures*
770 Primary cortical neurons were dissociated from mouse (C57BL/6J, The Jackson Laboratory)
771 E16.5 embryonic cortices into single cell suspensions with a papain dissociation system
772 (Worthington Biochemical Corporation). Tissue culture plates were coated with poly-L-lysine
773 (0.1% w/v) before seeding cells. Neurons were grown in Neurobasal media (Gibco)

774 supplemented with B-27 serum free supplement (Gibco), GlutaMAX (Gibco), and penicillin-
775 streptomycin (Gibco) in a humidified incubator at 37 °C, with 5% CO2. Half media changes
776 were performed every 4-5 days. Primary astrocytes were dissociated from P0-P1 mouse cortices
777 using the same papain dissociation methods as neurons, except the single cell suspensions were
778 then plated onto tissue culture plates without poly-L-lysine in DMEM with 10% FBS and
779 penicillin-streptomycin. Primary astrocyte cultures were passaged using Accutase (Stemcell
780 Technologies).
781
782 *Primary Human T Cell Cultures*
783 Blood from healthy donors collected in leukoreduction system (LRS) chambers was separated by
784 Ficoll-Paque density gradient to obtain peripheral blood mononuclear cells (PBMCs). $CD4^{pos}$
785 and $CD8^{pos}$ T cells were isolated by negative selection using EasySep Human CD4+ T Cell
786 Isolation Kit and EasySep Human CD8+ T Cell Isolation Kit (STEMCELL Technologies),
787 respectively, according to the manufacturer's instructions. T cells were cultured for 3 days with
788 CD3/CD28 Dynabeads (ThermoFisher Scientific) with 40 IU/mL IL-2 and spinoculated with
789 lentivirus for 2 hours at 400 rcf in the presence of 8 µg/mL polybrene. T cells were expanded
790 following transduction for two days in the presence of CD3/CD28 Dynabeads and 300 IU/mL
791 IL-2 prior to use in assays. Transduced or untransduced $CD4^{pos}$ or $CD8^{pos}$ T cells were co-
792 cultured for 24 hours together with A549 cells. Following co-culture, cells were harvested,
793 stained with antibodies against CD45, CD4, or CD8 (BioLegend) and analyzed on a
794 LSRFortessa flow cytometer (BD Biosciences). Each condition was run in triplicate, and two
795 independent experiments were conducted using T cells from different donors. For microscopy,

796 A549 cells were co-cultured with CD4 $^{pos}$ T cells in glass-bottom plates (MatTek Corporation)

797 and imaged on an LSM 700 confocal microscope (Zeiss).

798
799
800
801
802 **REFERENCES**


803 Bendas, G., and Borsig, L. (2012). Cancer cell adhesion and metastasis: selectins, integrins, and
804 the inhibitory potential of heparins. International journal of cell biology *2012*.
805 Boisset, J.-C., Vivié, J., Grün, D., Muraro, M.J., Lyubimova, A., and Van Oudenaarden, A. (2018).
806 Mapping the physical network of cellular interactions. Nature methods *15*, 547-553.
807 Crespo, J., Sun, H., Welling, T.H., Tian, Z., and Zou, W. (2013). T cell anergy, exhaustion,
808 senescence, and stemness in the tumor microenvironment. Current opinion in immunology *25*,
809 214-221.
810 Deb, A. (2014). Cell–cell interaction in the heart via Wnt/β-catenin pathway after cardiac injury.
811 Cardiovascular research *102*, 214-223.
812 Dittmer, J., and Leyh, B. (2014). Paracrine effects of stem cells in wound healing and cancer
813 progression. International journal of oncology *44*, 1789-1798.
814 Dustin, M.L., and Choudhuri, K. (2016). Signaling and polarized communication across the T cell
815 immunological synapse. Annual review of cell and developmental biology *32*, 303-325.
816 Fridy, P.C., Li, Y., Keegan, S., Thompson, M.K., Nudelman, I., Scheid, J.F., Oeffinger, M.,
817 Nussenzweig, M.C., Fenyö, D., and Chait, B.T. (2014). A robust pipeline for rapid production of
818 versatile nanobody repertoires. Nature methods *11*, 1253.
819 Giladi, A., Cohen, M., Medaglia, C., Baran, Y., Li, B., Zada, M., Bost, P., Blecher-Gonen, R.,
820 Salame, T.-M., and Mayer, J.U. (2020). Dissecting cellular crosstalk by sequencing physically
821 interacting cells. Nature Biotechnology, 1-9.
822 Halpern, K.B., Shenhav, R., Massalha, H., Toth, B., Egozi, A., Massasa, E.E., Medgalia, C., David,
823 E., Giladi, A., and Moor, A.E. (2018). Paired-cell sequencing enables spatial gene expression
824 mapping of liver endothelial cells. Nature biotechnology *36*, 962-970.
825 Joyce, J.A., and Fearon, D.T. (2015). T cell exclusion, immune privilege, and the tumor
826 microenvironment. Science *348*, 74-80.
827 Kitadai, Y. (2010). Cancer-stromal cell interaction and tumor angiogenesis in gastric cancer.
828 Cancer Microenvironment *3*, 109-116.
829 Komohara, Y., and Takeya, M. (2017). CAFs and TAMs: maestros of the tumour
830 microenvironment. The Journal of pathology *241*, 313-315.
831 Konry, T., Sarkar, S., Sabhachandani, P., and Cohen, N. (2016). Innovative tools and technology
832 for analysis of single cells and cell–cell interaction. Annual review of biomedical engineering *18*,
833 259-284.
834 Kota, J., Hancock, J., Kwon, J., and Korc, M. (2017). Pancreatic cancer: Stroma and its current
835 and emerging targeted therapies. Cancer letters *391*, 38-49.

836 Langridge, P.D., and Struhl, G. (2017). Epsin-dependent ligand endocytosis activates Notch by
837 force. Cell *171*, 1383-1396. e1312.
838 Li, G., Bethune, M.T., Wong, S., Joglekar, A.V., Leonard, M.T., Wang, J.K., Kim, J.T., Cheng, D.,
839 Peng, S., and Zaretsky, J.M. (2019). T cell antigen discovery via trogocytosis. Nature methods *16*,
840 183.
841 Lim, K.H., Huang, H., Pralle, A., and Park, S. (2013). Stable, high-affinity streptavidin monomer
842 for protein labeling and monovalent biotin detection. Biotechnology and bioengineering *110*,
843 57-67.
844 Los, G.V., Encell, L.P., McDougall, M.G., Hartzell, D.D., Karassina, N., Zimprich, C., Wood, M.G.,
845 Learish, R., Ohana, R.F., and Urh, M. (2008). HaloTag: a novel protein labeling technology for
846 cell imaging and protein analysis. ACS chemical biology *3*, 373-382.
847 Meurette, O., and Mehlen, P. (2018). Notch signaling in the tumor microenvironment. Cancer
848 Cell *34*, 536-548.
849 Morsut, L., Roybal, K.T., Xiong, X., Gordley, R.M., Coyle, S.M., Thomson, M., and Lim, W.A.
850 (2016). Engineering customized cell sensing and response behaviors using synthetic notch
851 receptors. Cell *164*, 780-791.
852 Nagarsheth, N., Wicha, M.S., and Zou, W. (2017). Chemokines in the cancer microenvironment
853 and their relevance in cancer immunotherapy. Nature Reviews Immunology *17*, 559.
854 Nielsen, M.F.B., Mortensen, M.B., and Detlefsen, S. (2016). Key players in pancreatic cancer-
855 stroma interaction: Cancer-associated fibroblasts, endothelial and inflammatory cells. World
856 journal of gastroenterology *22*, 2678.
857 Orimo, A., and Weinberg, R.A. (2006). Stromal fibroblasts in cancer: a novel tumor-promoting
858 cell type. Cell cycle *5*, 1597-1601.
859 Ovcinnikovs, V., Ross, E.M., Petersone, L., Edner, N.M., Heuts, F., Ntavli, E., Kogimtzis, A.,
860 Kennedy, A., Wang, C.J., and Bennett, C.L. (2019). CTLA-4–mediated transendocytosis of
861 costimulatory molecules primarily targets migratory dendritic cells. Science immunology *4*,
862 eaaw0902.
863 Pasqual, G., Chudnovskiy, A., Tas, J.M., Agudelo, M., Schweitzer, L.D., Cui, A., Hacohen, N., and
864 Victora, G.D. (2018). Monitoring T cell–dendritic cell interactions in vivo by intercellular
865 enzymatic labelling. Nature *553*, 496.
866 Swartz, M.A., Iida, N., Roberts, E.W., Sangaletti, S., Wong, M.H., Yull, F.E., Coussens, L.M., and
867 DeClerck, Y.A. (2012). Tumor microenvironment complexity: emerging roles in cancer therapy
868 (AACR).
869 Tanenbaum, M.E., Gilbert, L.A., Qi, L.S., Weissman, J.S., and Vale, R.D. (2014). A protein-tagging
870 system for signal amplification in gene expression and fluorescence imaging. Cell *159*, 635-646.
871 Tsioris, K., Torres, A.J., Douce, T.B., and Love, J.C. (2014). A new toolbox for assessing single
872 cells. Annual review of chemical and biomolecular engineering *5*, 455-477.
873 Venkatesh, H.S., Morishita, W., Geraghty, A.C., Silverbush, D., Gillespie, S.M., Arzt, M., Tam, L.T.,
874 Espenel, C., Ponnuswami, A., and Ni, L. (2019). Electrical and synaptic integration of glioma into
875 neural circuits. Nature *573*, 539-545.
876 Yaron, A., and Sprinzak, D. (2012). The cis side of juxtacrine signaling: a new role in the
877 development of the nervous system. Trends in neurosciences *35*, 230-239.

878 Zeng, Q., Michael, I.P., Zhang, P., Saghafinia, S., Knott, G., Jiao, W., McCabe, B.D., Galván, J.A.,
879 Robinson, H.P., and Zlobec, I. (2019). Synaptic proximity enables NMDAR signalling to promote
880 brain metastasis. Nature *573*, 526-531.
881 Zhang, Y., and Liu, F. (2019). Multidimensional Single-Cell Analyses in Organ Development and
882 Maintenance. Trends in cell biology.
883

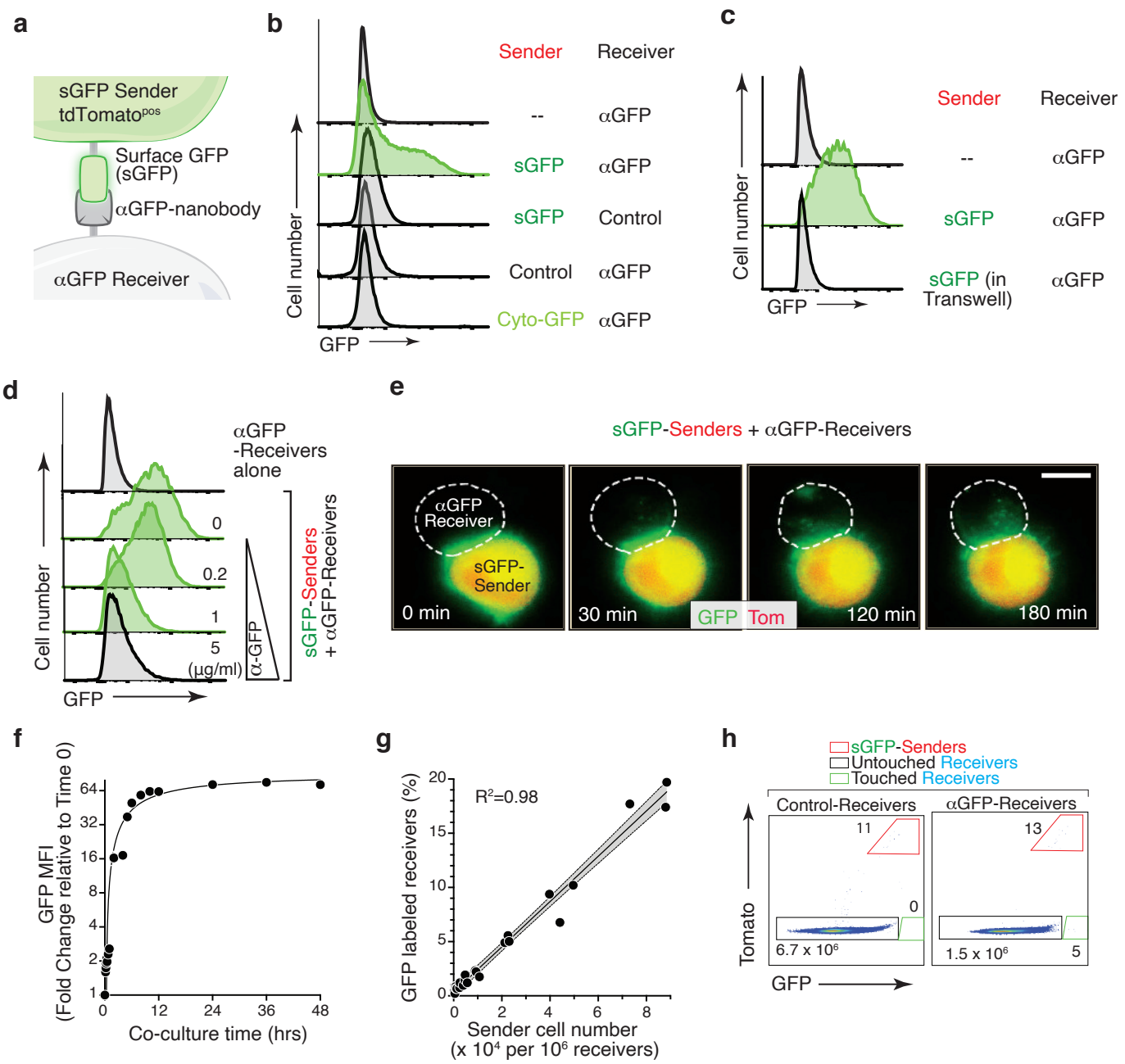


**Figure 1. GFP-based Touching Nexus (G-baToN) leads to cell-cell interaction-dependent receiver cell labeling**

**a.** Schematic of the G-baToN system. Surface GFP (sGFP) on a sender cell is transferred to a receiver cell expressing a cell surface anti-GFP nanobody (αGFP) leading to GFP labeling of the "touched" receiver.

**b.** GFP transfer from sGFP-expressing KPT lung cancer sender cells (marked by intracellular tdTomato) to αGFP-expressing 293 receiver cells. Receiver cell labeling is sGFP- and αGFP- dependent. Control sender cells do not express sGFP. Control receiver cells do not express αGFP. Cytoplasmic GFP (Cyto-GFP) is not transferred to receiver cells. Sender and receiver cells were seeded at a 1:1 ratio and co-cultured for 24 hours. Receivers were defined as Tomato$^{neg}$PI$^{neg}$ cells.

**c.** GFP transfer to 293 receiver cells requires direct cell-cell contact. Receiver cells separated from sender cells by a transwell chamber are not labeled. Sender and receiver cells were seeded in upper and lower chambers respectively at a 1:1 ratio and cultured for 24 hours. Receivers were defined as Tomato$^{neg}$PI$^{neg}$ cells.

**d.** GFP transfer to 293 receiver cells requires sGFP-αGFP interaction and is blocked by anti-GFP antibody in a dose-dependent manner. sGFP sender cells were pre-incubated with the indicated concentration of anti-GFP antibody for 2 hours, washed with PBS, and then co-cultured with receiver cells at a 1:1 ratio for 24 hours. Receivers were defined as Tomato$^{neg}$PI$^{neg}$ cells.

**e.** Time-lapse imaging of GFP transfer from a sGFP-expressing sender cell to an αGFP-expressing receiver cell. Time after contact is indicated. Receiver cell is outlined with white dashed line. Scale bar: 10 μm.

**f.** Analysis of GFP Mean Fluorescence Intensity (MFI) of αGFP receiver cells (marked by intracellular BFP) co-cultured with sGFP sender cells (marked by intracellular tdTomato) co-cultured for the indicated amount of time. Sender and receiver cells were seeded at a 1:1 ratio. Receivers were defined as Tomato$^{neg}$PI$^{neg}$BFP$^{pos}$ cells.

**g.** Percentage of labeled αGFP receiver cells after co-culture with different numbers of sender cells for 24 hours. Receivers were defined as Tomato$^{neg}$PI$^{neg}$BFP$^{pos}$ cells.

**h.** Detection of rare labeled αGFP receiver cells after co-culture with sGFP sender cells at approximately a 1:$10^5$ ratio for 24 hours. Receivers were defined as Tomato$^{neg}$PI$^{neg}$BFP$^{pos}$ cells.

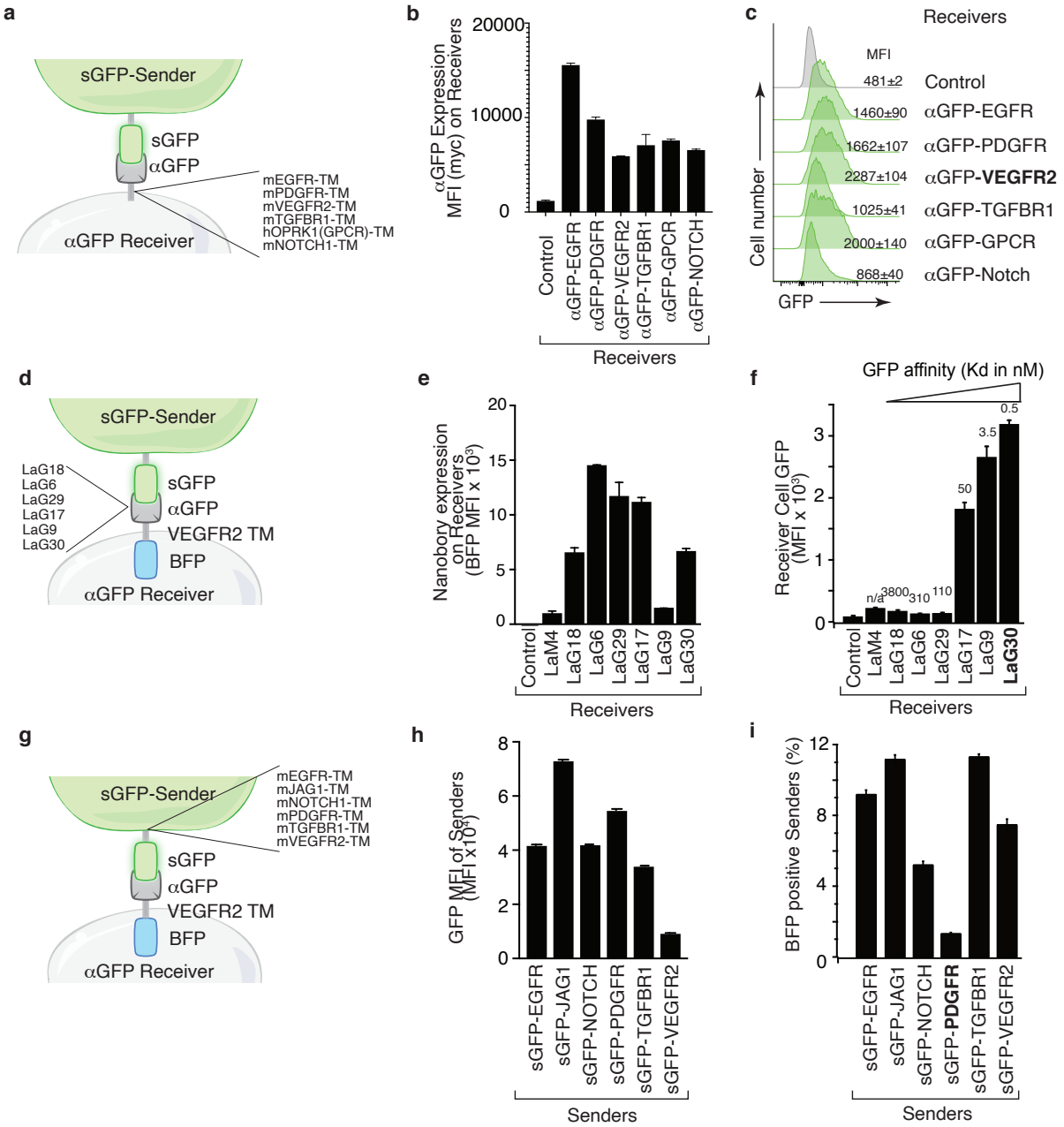


**Figure 2. Transmembrane domains and the nanobody affinity impact sGFP transfer and receiver cell labeling.**

**a**. Schematic of the sender and receiver cells used to determine the impact of different αGFP transmembrane (TM) domains. TM domains contain the TM domain itself as well as membrane proximal regions from the indicated mouse (m) and human (h) proteins.

**b.** Different TM domains impact cell surface αGFP expression on 293 receiver cells. Membrane αGFP was accessed by anti-Myc staining. Control receiver cells do not express any nanobody. Mean +/- SD of Myc MFI in triplicate cultures is shown.

**c.** VEGFR2 TM domain on αGFP receivers enables highest GFP transfer efficiency. Receiver cells expressing αGFP linked by different TM domains were co-cultured with sGFP sender cells at a 1:1 ratio for 6 hours. Receivers were defined as Tomato$^{neg}$PI$^{neg}$ cells.

**d.** Schematic of the sender and receiver cells used to determine the impact of different αGFP nanobodies on G-baToN-based labeling.

**e.** Different nanobodies exhibit different levels of expression on 293 receiver cells. Total αGFP expression was assessed by BFP intensity. Mean +/- SD of GFP MFI in triplicate cultures is shown.

**f.** αGFP affinity influences transfer of GFP to touched 293 receiver cells. Receiver cells expressing different αGFP nanobodies were co-cultured with sGFP sender cells at a 1:1 ratio for 6 hours. GFP transfer was assessed by flow cytometry. GFP intensity on Tomato$^{neg}$PI$^{neg}$BFP$^{pos}$ receiver cells is shown as mean +/- SD of triplicate cultures.

**d.** Schematic of the sender and receiver cells used to determine the impact of different sGFP TM domains on G-baTon-based labeling. TM domains contain the TM domain itself as well as membrane proximal regions from the indicated mouse (m) and human (h) proteins.

**g.** Different TM domains on sGFP impact its expression in 293 sender cells. sGFP expression in sender cells was assessed by flow cytometry for GFP. Mean +/- SD of GFP MFI in triplicate cultures is shown.

**h.** PDGFR TM domain on sGFP minimized retrograde transfer of αGFP from receiver cells to 293 sGFP sender cells. αGFP transfer to sGFP senders were determined as the percentage of mCherry$^{pos}$GFP$^{pos}$ sender cells that were also BFP$^{pos}$. Cells were co-cultured for 6 hours at a 1:1 ratio. Mean +/- SD of triplicate cultures is shown.

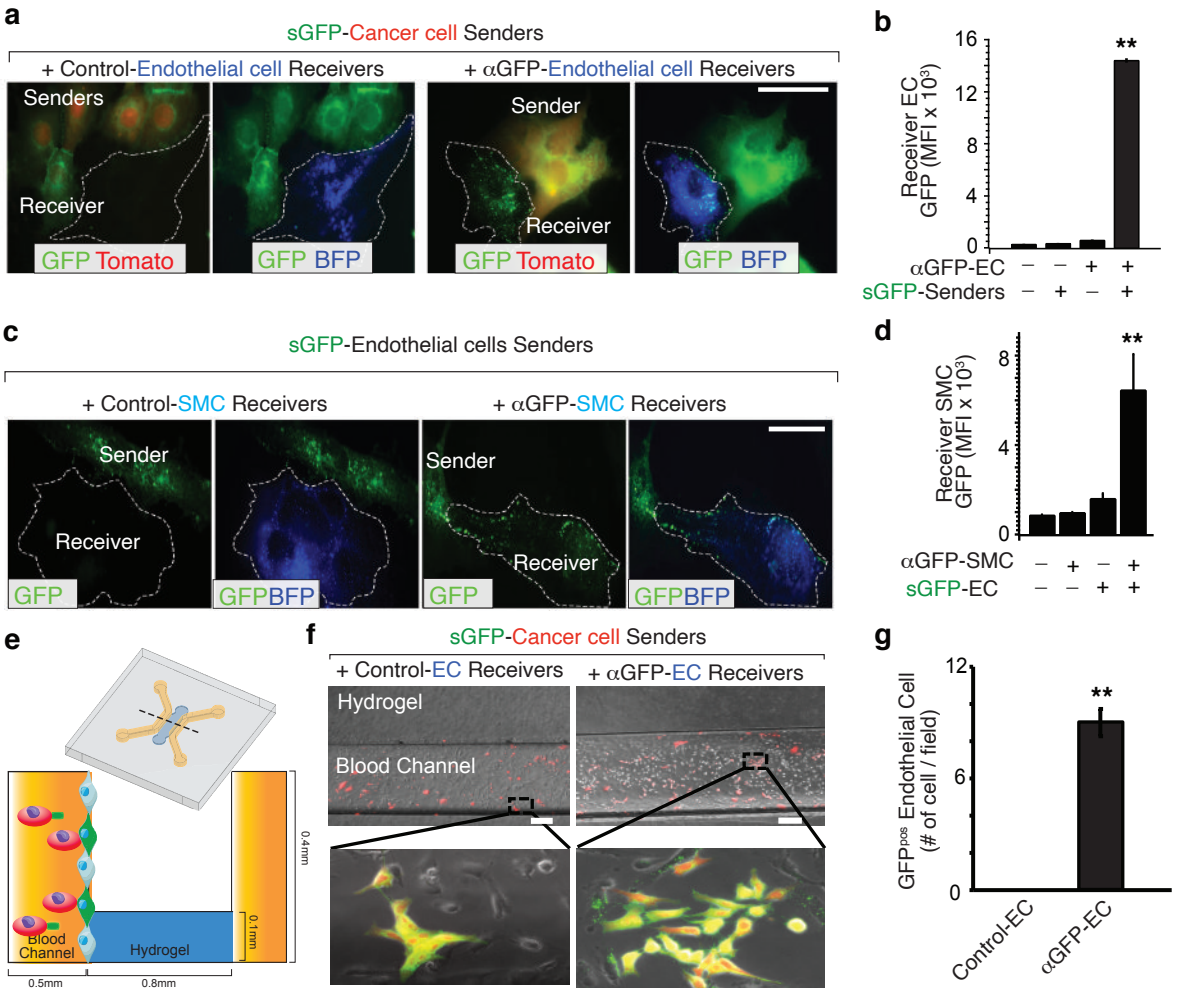


**Figure 3. G-baToN can be used for touching-based labeling between cancer cells and endothelial cells.**
**a, b.** G-baToN can detect cancer cell-endothelial cell (EC) interactions. HUVECs expressing αGFP were co-cultured with or without Tomato$^{pos}$ sGFP-expressing lung cancer sender cells at a 1:1 ratio for 24 hours. (**a**) Representative images of Tomato$^{pos}$ sGFP-expressing lung cancer sender cells co-cultured with either control HUVEC receiver cells (HUVECs expressing BFP) or αGFP HUVEC receiver cells at a 1:1 ratio for 24 hours . Scale bars = 50 µm. (**b**) MFI of GFP on PI$^{neg}$Tomato$^{neg}$BFP$^{pos}$CD31$^{pos}$ Receiver cells was assessed by flow cytometry and is shown as mean +/- SD of triplicate cultures. ** $p<0.01$, n=3.
**c,d.** G-baToN can detect endothelial cell (EC)-smooth muscle cell (SMC) interactions. Primary human umbilical artery smooth muscle cells (HUASMC) expressing αGFP were co-cultured with or without sGFP-expressing HUVEC senders cells at a 1:1 ratio for 24 hours. (**c**) Representative images of sGFP-expressing HUVEC sender cells co-cultured with either control HUASMC receiver cells (expressing BFP) or αGFP HUASMC receiver cells at a 1:1 ratio for 24 hours. Scale bars = 50 µm. (**d**) MFI of GFP on PI$^{neg}$BFP$^{pos}$ receiver cells was assessed by flow cytometry and is shown as mean +/- SD of triplicate cultures. ** $p<0.01$, n=3.
**e,f,g.** G-baToN can detect cancer cell-endothelial cell (EC) interactions in 3D-microfluidic culture. (**e**) Details on design of 3D-microfluidic devices for cancer cell-endothelial cell co-culture. (**f**) Representative images of Tomato$^{pos}$ sGFP-expressing lung cancer sender cells co-cultured with either control HUVEC receiver cells (HUVECs expressing BFP) or αGFP HUVEC receiver cells at a 1:10 ratio for 24 hours . Scale bars = 200 µm. (**g**) Average number of GFP$^{pos}$ hUVEC after co-culture with cancer cells for 24 h. 10 areas from three chips with 200X magnification were used for the quantification. ** $p<0.01$, n = 10.

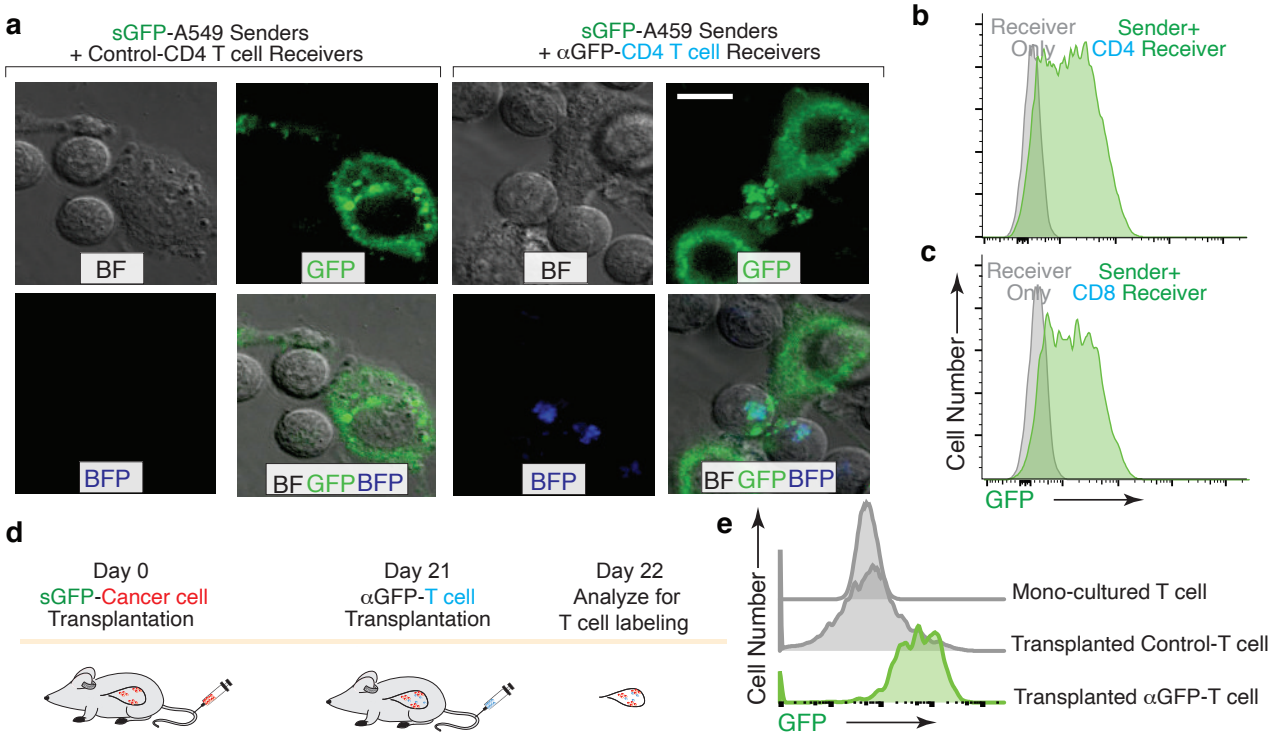


**Figure 4. G-baToN can detect T cells-cancer cells interactions.**
**a,b,c.** G-baToN can detect cancer cell-T cell interactions *in vitro*. **(a)** Primary human $CD4^{pos}$ or $CD8^{pos}$ T cells were co-cultured with sGFP-expressing lung cancer sender cells (A549 cells) at a 2:1 ratio for 24 hours. Representative image of A549 cell and CD4 T cell interactions. Scale bars = 10 μ m.**(b,c)** A549 cells expressing sGFP can transfer GFP to αGFP primary human $CD4^{pos}$ **(b)** or $CD8^{pos}$ **(c)** T cells after co-culture at a 1:1 ratio for 24 hours. Receivers were defined as Near-$IR^{neg}BFP^{pos}CD4^{pos}/CD8^{pos}$ T cells.
**d,e.** G-baToN can detect cancer cell-T cell interactions *in vivo*. **(d)** Experiment design for cancer cell-T cell interactions *in vivo*. $1X10^6$ sGFP-expressing lung cancer sender cells were transplanted into NSG mice at day 0. $4X10^6$ αGFP primary human $CD4^{pos}$ T cell were transplanted into tumor-bearing mice at day 21. 1 day after T cell transplantation (day 22), T cells in mouse lung were analyzed via FACS. **(e)** sGFP-expressing cancer cell can transfer GFP to αGFP-expressing primary human $CD4^{pos}$ T cells. Receives were defined as $PI^{neg}BFP^{pos}CD4^{pos}$T cells.

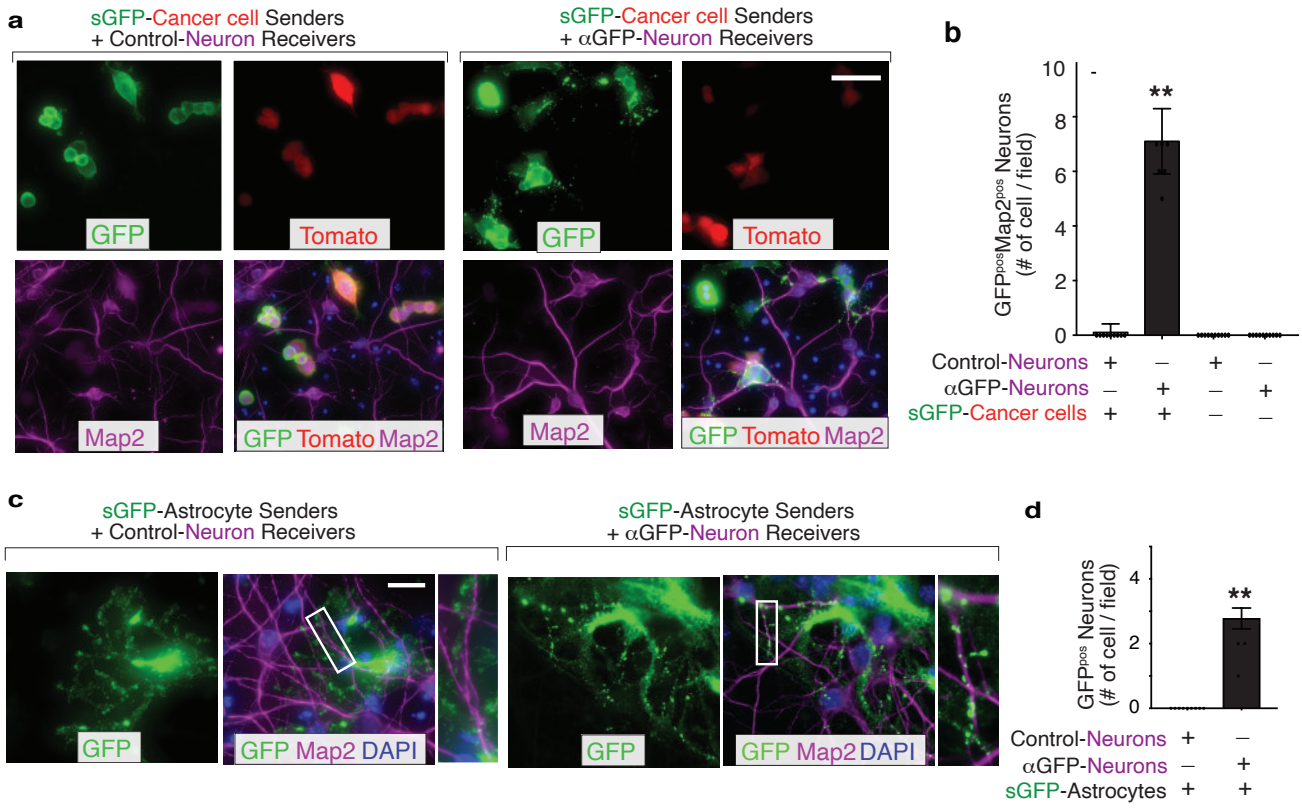


**Figure 5. G-baToN can detect neuron-cancer cell, neuron-astrocyte interactions.**
**a.** Representative image of sGFP-expressing cancer sender cells co-cultured with either control neuron receivers or αGFP neuron receivers at a 1:1 ratio for 24 hours. Neurons were stained with Microtubule Associated Protein 2 (Map2). Scale bars = 50 µm.
**b.** Quantification of supplementary Figure 5a using images from 10 different fields. Each dot represents a field. The bar indicates the mean +/- SD. $GFP^{pos}$ neurons were defined as $Map2^{pos}tdTomato^{neg}$ cells with GFP. ** $p<0.01$, n=10.
**c.** Representative images of sGFP-expressing astrocyte sender cells co-cultured with either control neuron receivers or αGFP neuron receivers at a 1:2 ratio for 24 hours. Neurons were stained with Map2. Scale bars = 50 µm. Higher magnification of the boxed areas are shown on the right.
**d.** Quantification of Figure 5c using images from 10 different fields. Each dot represents a field. The bar indicates the mean +/- SD. $GFP^{pos}$ neurons were defined as $Map2^{pos}$ cells with GFP. ** $p<0.01$, n=10.

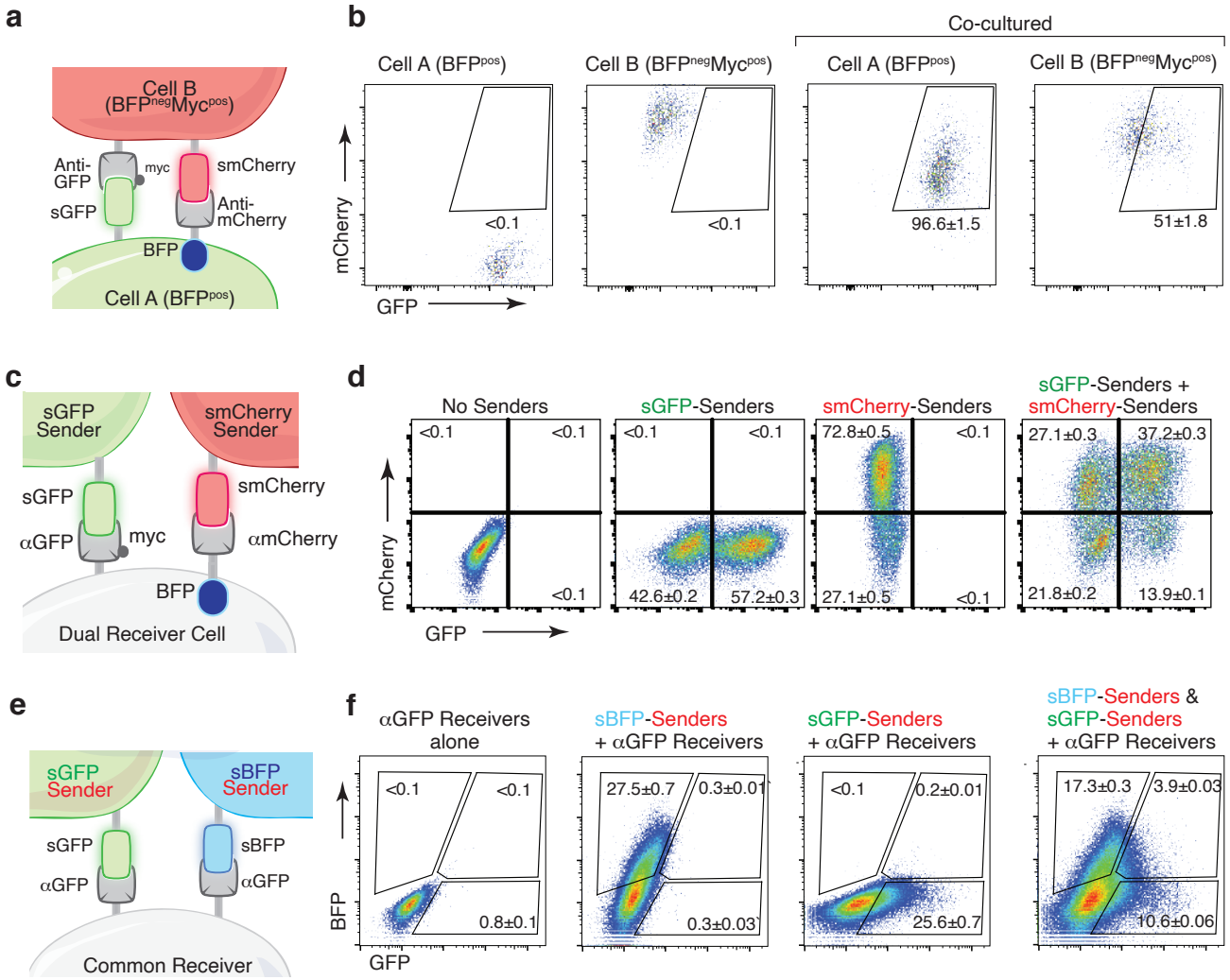


**Figure 6. Multicolor-baToN systems enable recording of higher order interactions.**

**a.** Diagram of the Reciprocal-baToN system. Cell A expresses sGFP and αmCherry (tagged by intracellular BFP), Cell B expresses smCherry and αGFP (tagged by Myc-tag).

**b.** Representative FACS plots of cell A and cell B monocultures (left 2 panels) and after co-culture at a 5:1 ratio for 24 hours. Percent of labeled cells is indicated as mean +/- SD of triplicate cultures.

**c.** Schematic of the AND gate-baToN system. sGFP and smCherry sender cells express either sGFP or mCherry. Dual receiver cells express both αGFP (LaG17, tagged by Myc-tag) and αmCherry (LaM4, tagged by intracellular BFP).

**d.** Representative FACS plots of dual receiver 293 cells cultured with the indicated 293 sender cells at 1:1 (for single sender cell) or 1:1:1 (for dual sender cells) ratios. Percent of labeled receiver cells (gated as $BFP^{pos}$) after 24 hours of co-culture is indicated as mean +/- SD of triplicate cultures.

**e.** Diagram of the BFP/GFP AND gate-baToN system. sBFP sender cells express intracellular Tomato and surface BFP, sGFP sender cells express intracellular Tomato and surface GFP. Common receiver cells expressed αGFP.

**f.** Representative FACS plots of common receiver 293 cells cultured with the indicated $Tomato^{pos}$ sender cells at 1:1 (for single sender cell) or 1:1:1 (for dual sender cells) ratios. Receiver cells were gated as $Tomato^{neg}PI^{neg}$. Percent of labeled common receiver cells after 24 hours of co-culture is indicated as mean +/- SD of triplicate cultures.

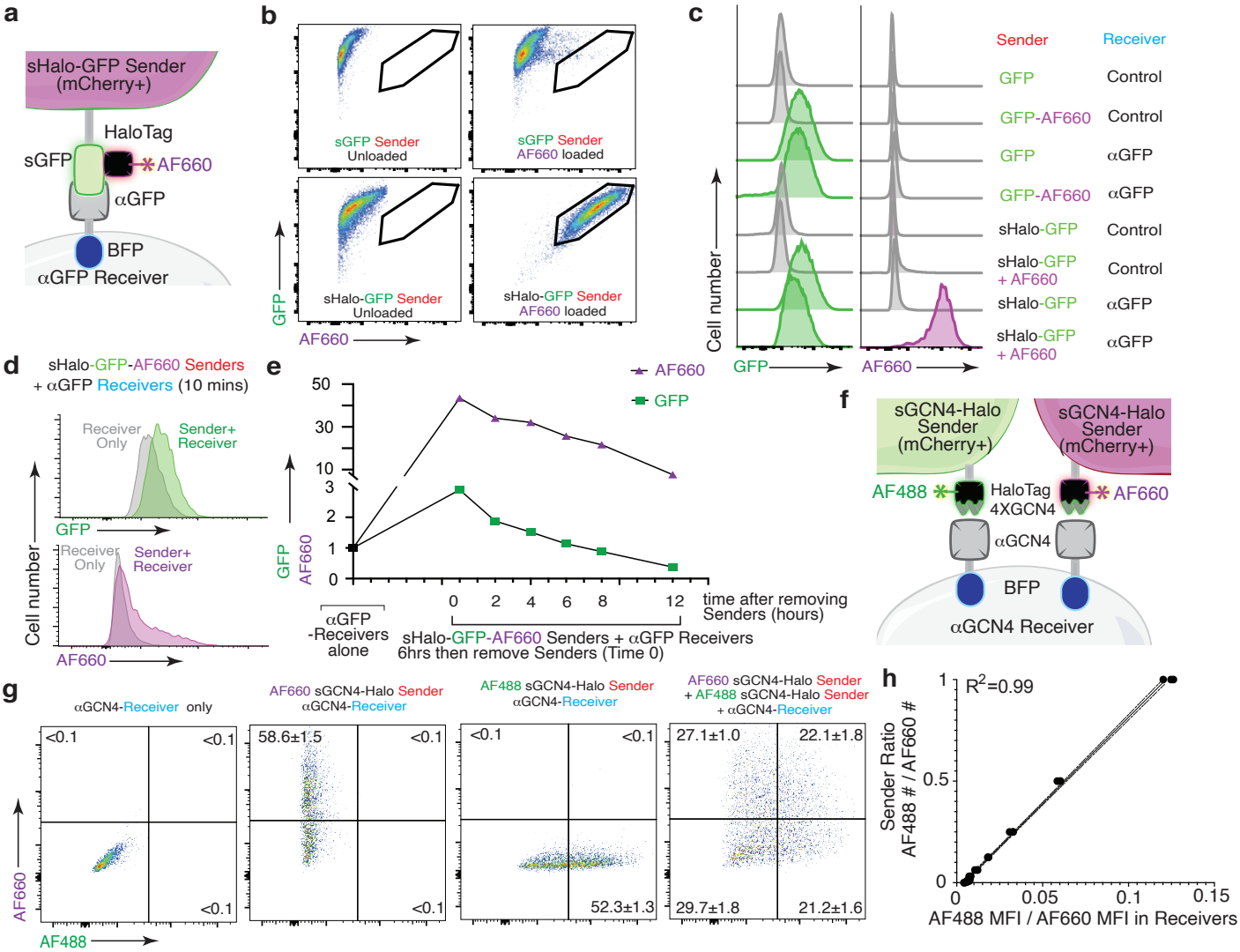


**Figure 7. HaloTag-baToN systems enable quantitative and sensitive cell-cell interaction-dependent receiver cell labeling.**
**a.** Diagram of HaloTag-baToN system. Sender cells (marked by intracellular 2A-mCherry) express surface HaloTag-GFP fusion which can be loaded with HaloTag ligands (in this example AF660). Receiver cells express αGFP (LaG17, tagged by intracellular BFP).
**b.** Labeling HaloTag-expressing sender cells with AF660 fluorophore. Representative FACS plots of KP (lung adenocarcinoma) sender cells expressing either sGFP or sGFP-sHaloTag incubated with AF660-conjugated HaloTag ligand for 5 minutes on ice. AF660 specifically labeled sHaloTag-GFP sender cells but not sGFP sender cells.
**c**. Representative histogram of GFP and AF660 intensity in αGFP 293 receiver cells cultured with HaloTag-GFP sender cells at a 1:1 ratio for 6 hours. Receivers were defined as $mCherry^{neg}PI^{neg}BFP^{pos}$ cells.
**d**. AF660 transfer to αGFP 293 receiver cell is rapid after cell-cell interaction. AF660 MFI shift was detected after mixing sHalo-GFP senders and αGFP receivers and co-culture for 10 minutes. AF660 MFI shift was more dramatic than GFP. Receivers were defined as $mCherry^{neg}PI^{neg}BFP^{pos}$ cells.
**e**. Slower AF660 quenching in touched receiver cells after removing sHalo-GFP senders. After 6 hours co-culture, GFP/AF660 positive receiver cells were purified via FACS. Analysis of GFP/AF660 MFI in purified receiver cells showed rapid GFP degradation but slower AF660 quenching. Receivers were defined as $mCherry^{neg}PI^{neg}BFP^{pos}$ cells.
**f.** Diagram of dual color GCN4-HaloTag-baToN system. Sender cells (marked by intracellular 2A-mCherry) express surface 4XGCN4 associated with HaloTag, loaded with either AF488- or AF660- conjugated HaloTag ligand. Receiver cells express αGCN4 (tagged by intracellular BFP).
**g.** Representative FACS plots of αGCN4 receiver cells co-cultured with the indicated sender cells at 1:1 (for single sender cell) or 1:1:1 (for dual sender cells) ratios. Percent of labeled receiver cells (gated as $mCherry^{neg}PI^{neg}BFP^{pos}$) after 6 hours of co-culture is indicated as mean +/- SD of triplicate cultures.
**h.** AF488/AF660 GCN4-HaloTag sender ratio in the co-culture directly proportional to AF488/AF660 intensity (MFI) of αGCN4 receiver after 6 hours of co-culture. Receivers were defined as $mCherry^{neg}PI^{neg}BFP^{pos}$ cells.

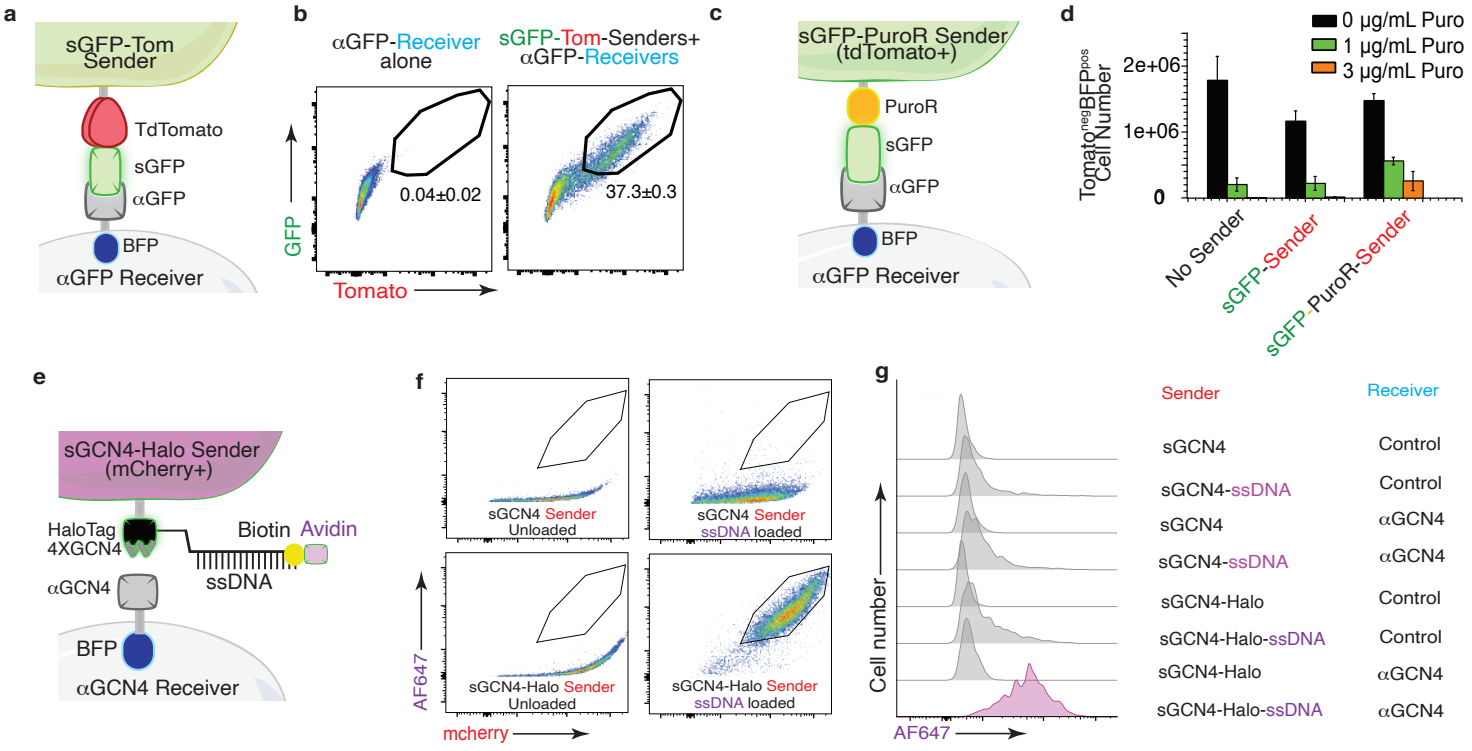


**Figure 8. The G-baToN system can co-transfer cargo molecules into touched receiver cells.**

**a**. Diagram of surface tdTomato-GFP (sGFP-Tom) co-transfer into touched receiver cells. Sender cell expresses sGFP-tdTomato and receiver cell expresses αGFP (tagged by intracellular BFP).

**b**. Representative FACS plots of αGFP 293 receiver cells cultured with the indicated sender cells at 1:1 ratio for 24 hours. Percent of GFP/Tomato dual labeled receiver cells is indicated as mean +/- SD of $BFP^{pos}$ cells from triplicate cultures.

**c**. Diagram of GFP-PuroR co-transfer system. Sender cell expresses surface GFP associated with PuroR (marked by intracellular tdTomato), receiver cell expresses αGFP (tagged by intracellular BFP). PuroR: Gcn5-related N-acetyltransferase.

**d**. Co-transfer of GFP-PuroR from sGFP-PuroR sender cells to αGFP 293 receiver cells confers puromycin resistance to receiver cells. Control, sGFP or sGFP-PuroR sender cells were co-cultured with αGFP 293 receiver cells for 24 hours at a 4:1 ratio before treatment with different dose of puromycin for 48 hours. $tdTomato^{neg}PI^{neg}BFP^{pos}$ cell numbers were counted via FACS.

**e.** Diagram of using GCN4-HaloTag sender to transfer ssDNA into αGCN4 receiver cells. Sender cells (marked by intracellular 2A-mCherry) express surface 4XGCN4 associated with HaloTag, loaded with 5' HaloTag ligand, 3' biotin dual conjugated ssDNA (21 nt), then stained with Avidin-AF647. Receiver cells express αGCN4 (tagged by intracellular BFP).

**f.** Loading of sender cells with ssDNA. Representative FACS plots of 293 sender cells expressing either sGCN4 or sGCN4-Halo were loaded with 5' HaloTag-ligand, 3' biotin dual conjugated ssDNA (21nt), then stained with Avidin-AF647. AF647 specifically labeled loaded sGCN4-Halo sender cells but not sGCN4 sender cells.

**g.** Representative plot of AF647 intensity in αGCN4 293 receiver cells co-cultured with GCN4-HaloTag 293 sender cells at a 1:1 ratio for 6 hours. Receivers were defined as $mCherry^{neg}PI^{neg}BFP^{pos}$ cells.

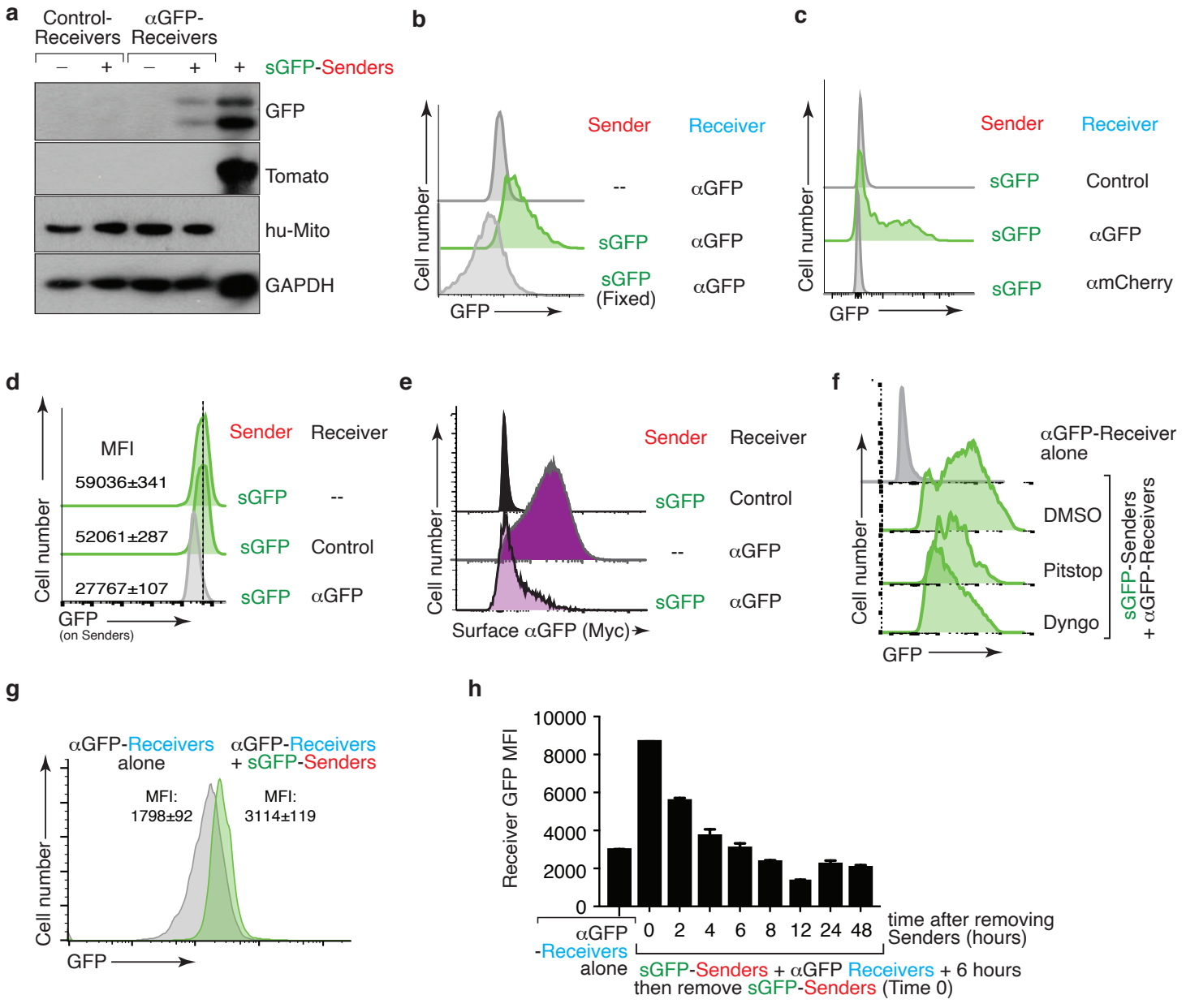


**Supplementary Figure 1. GFP transfer requires direct GFP-αGFP interaction.**

**a.** GFP protein is transferred to receiver cells. Western blot analysis of FACS purified Control and αGFP receiver 293 cells cultured in isolation or co-culture with sGFP Tomato-positive sender cells (mouse KPT lung cancer cells) for 24 hours. sGFP but not Tomato is present in touched αGFP receiver cells. Human mitochondrial antigen (hu-Mito) is a marker for receiver cells. GAPDH shows loading. Rightmost lane is sGFP sender cells.

**b.** GFP cannot be transferred from fixed sGFP sender cells to live αGFP receiver cells. sGFP sender cells were fixed in 1% PFA for 5 minutes and washed with PBS before co-cultured with αGFP receiver cells at a 1:1 ratio for 24 hours. Receivers were defined as $Tomato^{neg}PI^{neg}BFP^{pos}$ cells.

**c.** GFP transfer to 293 receiver cells required sGFP-αGFP recognition. GFP is transferred from sGFP sender cells to αGFP-receiver cells but not from sGFP sender cells to αmCherry-receiver cells. Control receiver cells do not express any nanobody. Sender and receiver cells were co-cultured at a 1:1 ratio for 24 hours. Receivers were defined as $Tomato^{neg}PI^{neg}BFP^{pos}$ cells.

**d.** GFP transfer to receiver cells is accompanied by a reduction of GFP on the sender cells. GFP expression on sender cells after 24 hour co-culture with control or αGFP-expressing 293 receiver cells at a 1:1 ratio. Co-culture with αGFP expressing but not control receiver cells reduced GFP on sGFP sender cells. Senders were defined as $Tomato^{pos}DAPI^{neg}BFP^{neg}$ cells.

**e.** GFP transfer is accompanied with αGFP internalization on receiver cells. Analysis of surface αGFP (Myc-tag) on 293 receiver cell co-cultured for 24 hours with sGFP sender cells. Receivers were defined as $Tomato^{neg}PI^{neg}$ cells.

**f.** GFP transfer to 293 receiver cells is partially dependent on membrane dynamics of endocytosis. Both a clathrin inhibitor (Pitstop, 20 μM) and a dynamin inhibitor (Dyngo 4a, 10 μM) partially inhibit GFP transfer from sGFP sender cells to αGFP receivers. Inhibitors were present during the 24 hour co-culture. Receivers were defined as $Tomato^{neg}PI^{neg}$ cells.

**g.** GFP transfer to αGFP 293 receiver cells can be very rapid. A shift in GFP MFI was detected 5 minutes after mixing sGFP sender cells with αGFP receiver cell. Receivers were defined as $Tomato^{neg}PI^{neg}BFP^{pos}$ cells. MFI mean +/- SD of triplicate cultures is shown.

**h.** Rapid GFP degradation in touched receiver cells after removal of the sGFP sender cells. After 6 hours co-culture, GFP positive receiver cells were purified by FACS followed by culture without sender cells. Receivers were defined as $mCherry^{neg}PI^{neg}BFP^{pos}$ cells. GFP MFI in receiver cells reduced rapidly ($T_{1/2}$ approximately 2 hours). MFI mean +/- SD of triplicate cultures is shown.

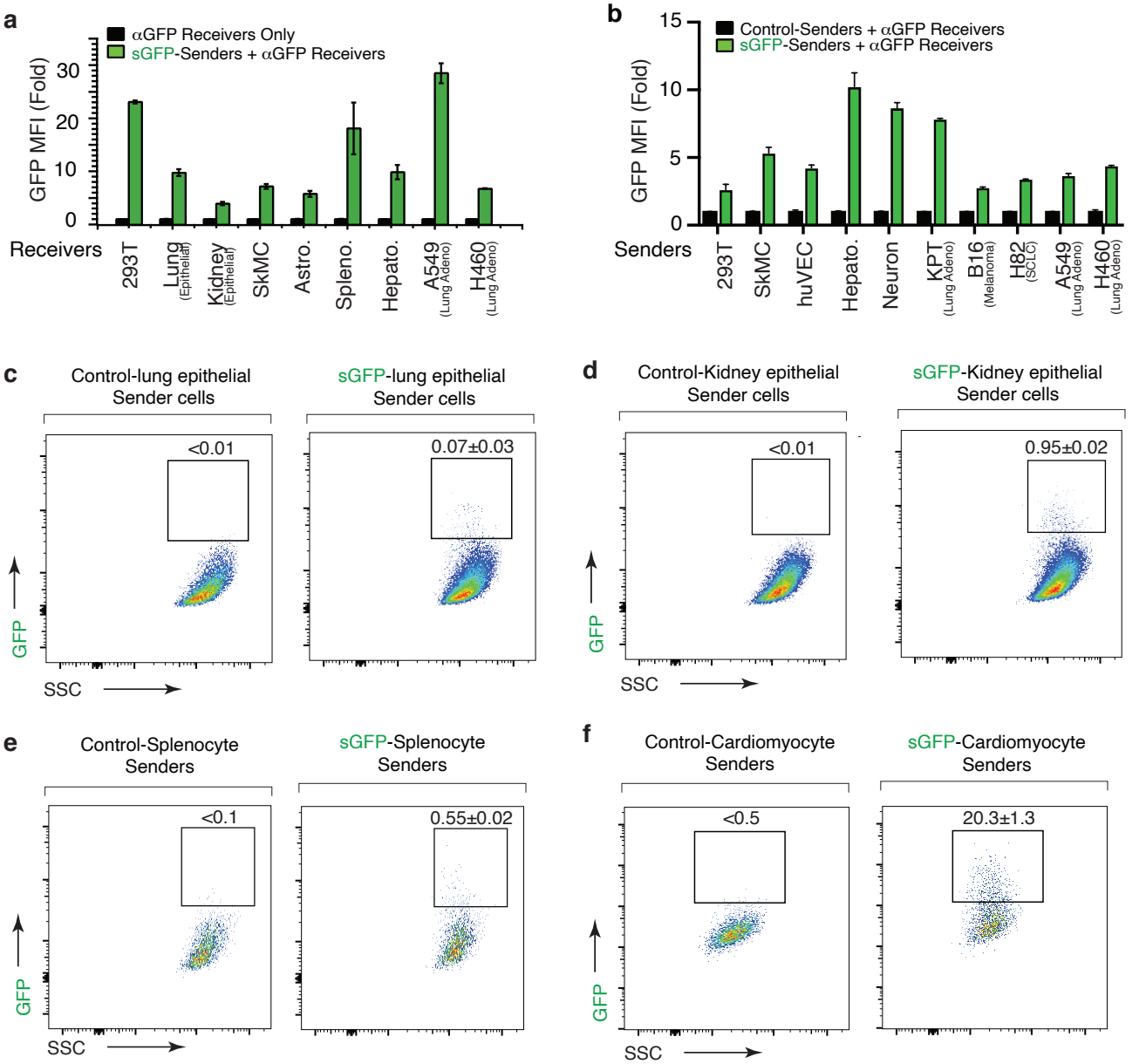


**Supplementary Figure 2. G-baToN is a generalized system that can be used for touching-based labeling between various cell types.**
**a**. Many different cell lines and primary cell types can serve as receiver cells. Receiver cells expressing αGFP were co-cultured with sGFP-expressing KPT sender cells for 24 hours. MFI of GFP on Tomato$^{neg}$PI$^{neg}$BFP$^{pos}$ receiver cells was assessed by FACS analysis and is shown as fold change relative to monocultured receiver cells. For lung epithelial cells and kidney epithelial cells MFI of GFP on Tomato$^{neg}$PI$^{neg}$BFP$^{pos}$EpCAM$^{pos}$ cells is shown as mean +/- SD of triplicate cultures. SkMC: skeletal muscle cells. Astro: Astocytes. Hepato: hepatocytes. Spleno: splenocytes.
**b.** Many different cell lines and primary cell types can serve as sender cells. Sender cells expressing sGFP were co-cultured with αGFP 293 receiver cells for 24 hours. MFI of GFP on mCherry$^{neg}$PI$^{neg}$BFP$^{pos}$ receiver cells was assessed by flow cytometry and is shown as fold change relative to monocultured 293 receiver cells. Mean +/- SD of triplicate cultures is shown.
**c,d,e,f.** Diverse primary mouse cells expressing sGFP can transfer GFP to αGFP 293 receivers. Different primary sender cells were first sorted based on their cell surface markers, then transduced with lentiviral vectors expressing sGFP before being co-cultured with αGFP 293 receiver cells for 24 hours. Percentage of mCherry$^{neg}$PI$^{neg}$BFP$^{pos}$GFP$^{pos}$ receiver cells was assessed by flow cytometry. For each primary sender, approximate sGFP$^{pos}$ sender : αGFP$^{pos}$ receiver ratio is indicated: **c.** Lung epithelial cells (1:180) (sorted EpCam$^{pos}$ cells from dissociated adult lung); **d**. Kidney epithelial cells (1:20) (sorted EpCam$^{pos}$ cells from dissociated adult kidney); **e**. Splenocyte (1:20); **f**. Cardiomyocyte (1:5) (sorted Sirpa$^{pos}$ cells from dissociated adult heart). Percent of labeled cells is indicated as mean +/- SD of triplicate cultures.

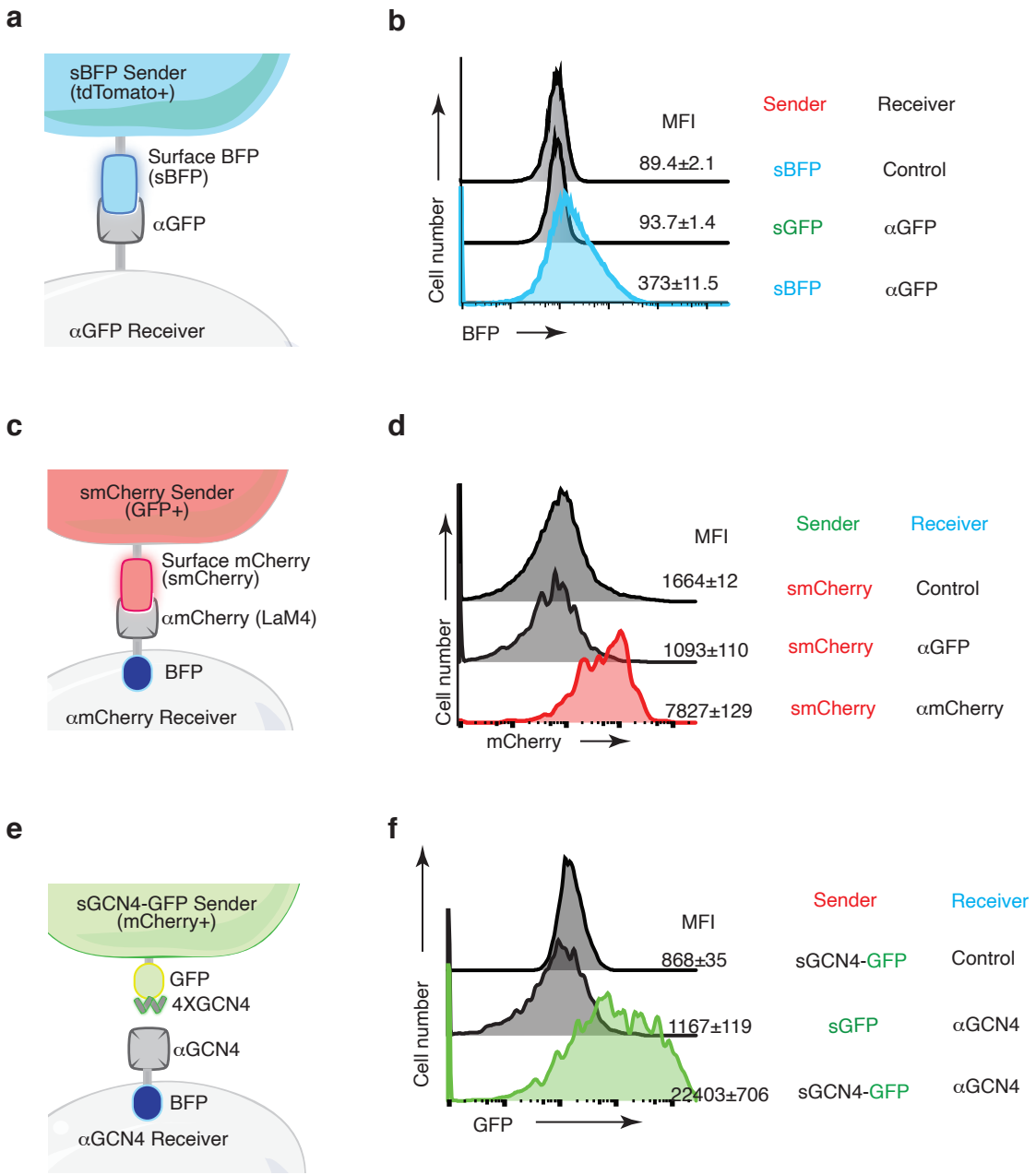


**Supplementary Figure 3. X-baToN systems enable fluorescent labeling via various antigen-nanobody/scFV pairs.**
**a.** Schematic of the surface BFP (sBFP)-baToN system. Sender cell (marked by intracellular tdTomato) expresses sBFP and receiver cell expresses α GFP.
**b.** The cross reactivity of αGFP with BFP allow BFP to be transferred from sBFP sender to αGFP receiver cells. sBFP senders and αGFP receivers were co-cultured at 1:1 ratio for 24 hours. Receivers were defined as toTomato$^{neg}$PI$^{neg}$ cells. BFP MFI of receiver cells is shown as mean +/- SD of triplicate cultures.
**c.** Schematic of the surface mCherry (smCherry)-baToN system. Sender cell (marked by intracellular GFP) expresses smCherry and receiver cell expresses αmCherry (tagged by intracellular BFP)
**d.** The pairing between mCherry and αmCherry enable mCherry transfer from smCherry 293 Sender cells to αmCherry-expressing 293 Receiver cells. smCherry senders are not able to transfer mCherry to αGFP receiver cells. smCherry sender cells were co-cultured with αGFP or αmCherry receiver cells at a 1:1 ratio for 24 hours. Receivers were defined as GFP$^{neg}$BFP$^{pos}$ cells. mCherry MFI of receiver cell is shown as mean +/- SD of triplicate cultures. smCherry 293 sender is not able to transfer mCherry to αGFP 293 receiver.
**e.** Schematic of the surface GCN4 (sGCN4)-baToN system. Sender cells (marked by intracellular 2A-mCherry) express cell surface 4X GCN4 peptide fused with GFP. Receiver cells express a cell surface anti-GCN4 single-chain variable fragment (scFV; αGCN4, tagged by intracellular BFP).
**f.** The pairing between GCN4 and αGCN4 enables co-transfer of GFP from 4X sGCN4-GFP senders to αGCN4 receivers 24 hours after co-culture at a 1:1 ratio. Receivers were defined as mCherry$^{neg}$PI$^{neg}$BFP$^{pos}$ cells. GFP MFI of receiver cell is shown as mean +/- SD of triplicate cultures. sGFP sender are not able to transfer GFP to αGCN4 receivers.

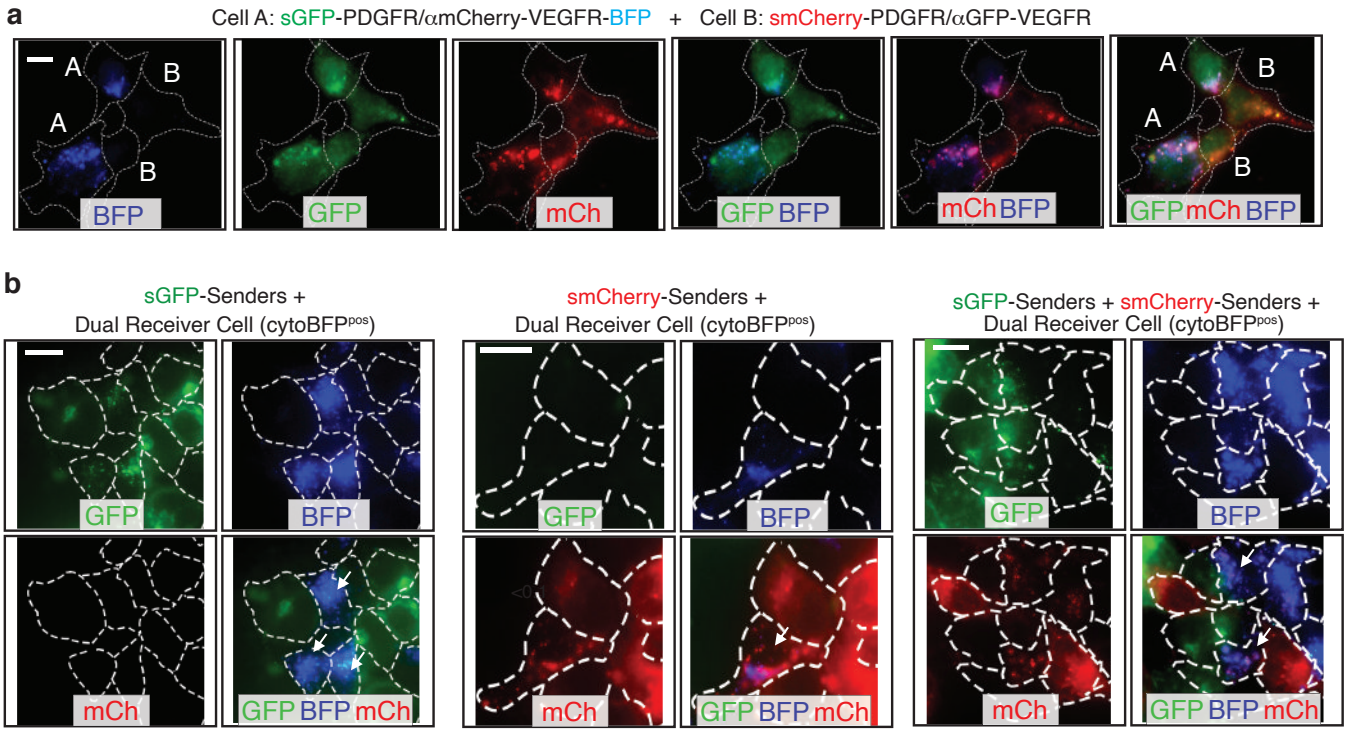


**Supplementary Figure 4. Dual color-baToN systems enable labeling in complex cell-cell interaction systems.**
**a.** Representative image of reciprocal labeling of cell A and cell B co-cultured for 24 hours. Cells are outlined with a white dashed line. Cell A is BFP and GFP double positive and Cell B is mCherry positive. Touched cell A is BFP, GFP and mCherry triple positive and touched cell B is GFP and mCherry double positive (pointed out by white letter). Scale bar: 10 µm.
**b**. Representative image of dual receiver cells co-cultured with indicated sender cells. Cells are outlined with a white dashed line. Dual receiver cells are BFP positive and sender touched dual receiver cells are pointed out by white arrows. Scale bar: 10 µm.

| | **synNotch** (Morsut *et al.*, Cell, 2016) | **LIPSTIC** (Pasqual *et al.*, Nature, 2018) | **G-baToN** (This manuscript) |
|---|---|---|---|
| **Cell-cell interaction** | 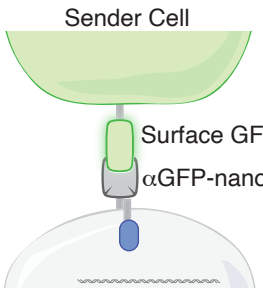  | 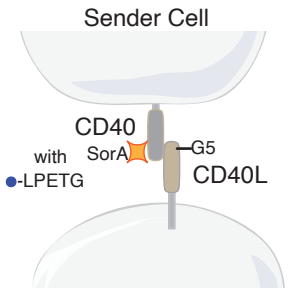  | 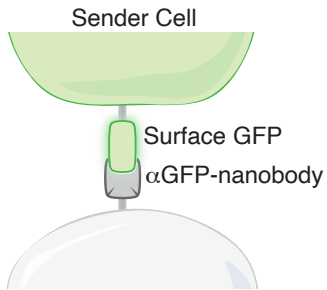  |
| **Receiver Cell after interaction** | 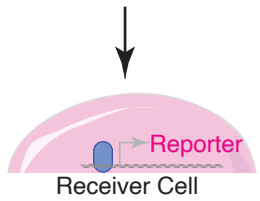  | 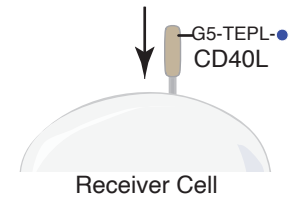  | 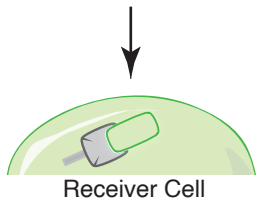  |
| **Basis of the labeling** | Notch intracellular cleavage leads to transcription factor release and activation of a reporter | Covalent labeling of receptor by ligand associated enzyme | Ligand internalization |
| **Additional requirement for labeling** | Engineered reporter in receiver cells | Labeling substrate | None |
| **Determinants of label half-life after touching** | Transcription factor half-life and reporter mRNA and protein half-life in the receiver cell | Labeled protein half-life on the receiver cell | Half-life of transferred protein or fluorophore in the receiver cell |
| **Advantages** | Generic sender and receivers<br>Generalizable across cell type<br>Compatable with AND gates<br>Tf can drive expression of many genes of interest | Requirement for exogenous substrate adds temporal control of labelling<br>Conceptually generalizable to other receptor ligand pairs | Simple two-component system<br>Low background<br>Single cell level sensitivity<br>Generalizable across cell type<br>Generic sender and receivers<br>Complex cell-cell interactions |
| **Potential disadvantages** | Engineered ligand-receptor interactions could influence cell-cell contact<br>Background activation or reporter could be leaky | Requires knowledge of receptor-ligand interactions between cell types of interest | Engineered ligand-receptor interactions could influence cell-cell contact |

**Supplementary Figure 5. Features of the synNotch, LIPSTIC, and G-BaToN cell-cell interaction reporter systems.**
Overview of systems that enable labeling of cells after cell-cell contact.